

**Staphylococci planktonic and biofilm environments differentially affect macrophage immune activation and osteoclastogenic differentiation.**

**Running title: Effect of biofilm formation on macrophage function.**

Elisabeth Seebach<sup>1\*</sup>, Tabea Elschner<sup>1</sup>, Franziska V. Kraus<sup>2</sup>, Margarida Souto-Carneiro<sup>2</sup> and Katharina F. Kubatzky<sup>1\*</sup>

1 Department of Infectious Diseases, Medical Microbiology and Hygiene, University Hospital Heidelberg

(Im Neuenheimer Feld 324, 69120 Heidelberg, Germany)

2 Department of Rheumatology, Medical Clinic 5, University Hospital Heidelberg

(Im Neuenheimer Feld 410, 69120 Heidelberg, Germany)

\*Corresponding authors

E-mail address:

elisabeth.seebach@med.uni-heidelberg.de

kubatzky@uni-heidelberg.de

## **Abstract (250 words)**

Implant-related bone infections are a major complication in orthopedic surgery that lead to inflammation and bone destruction. Bacterial biofilm formation on the implant is discussed to polarize the immune response towards tolerance and to facilitate bacterial persistence. In addition to their role in the early immune response, macrophages are osteoclast precursor cells. Therefore, macrophages can link inflammation and RANKL-mediated osteoclastogenic bone destruction.

We investigated the influence of *Staphylococcus aureus* (SA) and *epidermidis* (SE) biofilm formation on immune function and osteoclastogenesis using RAW264.7 cells and conditioned media (CM) of planktonic and biofilm cultures in the presence and absence of the osteoclastogenic transcription factor RANKL. Analysis of immune cell activation, metabolic activity and osteoclast formation revealed that a planktonic environment causes a pro-inflammatory response. This was also partially induced by biofilm CM. Simultaneous stimulation with CM and RANKL suppressed osteoclast formation in favor of a long-term immune activation. While the early macrophage response towards CM was dominated by glycolysis, the CM and RANKL approach shifted metabolism towards increased mitochondrial biomass and activity. This was most evident in biofilm CM. We further showed that planktonic CM effects are mediated through activation of TLR signaling and induction of IFN- $\beta$  production. In biofilm CM, high lactate levels seem to significantly contribute to the modulation of macrophages.

Our results can contribute to find targets for therapeutic intervention that restore an effective pro-inflammatory immune response, which could help to control implant-related bone infections.

## **Importance (150 words)**

The number of endoprosthetic and bone reconstructive surgeries is rising and accordingly incidences of implant-related bone infections increase. Biofilm formation on the implant surface protects bacteria against most antibiotics and the host's immune response. Thus, novel therapeutic strategies for prevention or treatment of biofilm formation are needed. Furthermore, bone infections are associated with osteoclast-mediated bone destruction, which promotes infection progression and ultimately leads to implant loosening. We investigated the effect of staphylococci-mediated biofilm formation on macrophage immune activation and osteoclastogenic differentiation, respectively. In planktonic and biofilm environments, immune cell activation dominated over osteoclastogenesis. The effects of planktonic environments were mainly mediated through activation of TLR signaling and resulted in a pronounced pro-inflammatory and IFN- $\beta$  macrophage immune response. In biofilm environments, high lactate

levels impaired osteoclast formation but also prevented an effective long-term immune activation. Therefore, targeting biofilm-derived metabolites but also IFN- $\beta$  signaling might be promising novel treatment strategies.

## Keywords

Implant-related bone infections, *Staphylococcus*, biofilm, macrophages, immune response, osteoclastogenesis

## Introduction

Implant-related bone infections are a major complication in orthopedic and trauma surgery. They lead to tissue inflammation and osteoclast-mediated bone destruction with severe consequences for the patients including long-term antibiotic treatment, repeated surgeries, implant revision and at worst amputation of the infected limb (1, 2). Chronic progression of these infections is frequent, as bacteria can colonize the implant and form biofilms on its surface. Biofilms act as an impenetrable matrix and shield embedded bacteria against eradication by antibiotic treatment and host immune defense mechanisms (3-6). Several studies show that biofilms promote a more tolerant immune response, which allows bacterial persistence (7, 8).

*Staphylococcus aureus* (SA) and *epidermidis* (SE) are the most frequently isolated bacteria causing implant-related bone infections (1, 6). SA contains a broad range of virulence factors, is able to survive intracellularly and can form biofilms (9). The commensal SE relies on biofilm formation as an immune evasion strategy (10). Thus, SA is pre-dominantly found in early and acute infections associated with pain, swelling and fever and implicates a high risk for infection recurrence after antibiotic and surgical treatment (11). SE instead causes only mild symptoms and low-grade inflammation and by this is commonly detected only after chronicity of infections, which is closely linked to biofilm formation.

Macrophages are innate immune cells with an important role in the first line of defense against invading pathogens. In most infections together with other cells of the innate immune system, they are efficient to clear bacteria by phagocytosis and production of anti-microbial molecules such as nitric oxide (NO) species. Furthermore, macrophages are antigen-presenting cells that induce an adaptive immune response (12). *In vitro*, they can be polarized into pro-inflammatory (M1) and anti-inflammatory (M2) phenotypes (13). This classification is defined by the presence of specific surface markers, the expression of inducible nitric oxide synthase (iNOS, M1) or arginase 1 (Arg-1, M2) and the cytokine profile of the respective macrophage population (14).

Macrophage subtypes are also characterized by a different metabolic activity with M1 macrophages relying pre-dominantly on glycolysis and M2 macrophages being more associated with oxidative phosphorylation (OxPhos) (15). The biofilm environment is considered to support an anti-inflammatory macrophage polarization by promoting mitochondrial respiration and anti-inflammatory IL-10 gene expression (16).

In addition to their immune function, macrophages serve as precursor cells for bone resorbing osteoclasts. Osteoclastogenesis is induced by binding of receptor activator of NF- $\kappa$ B ligand (RANKL) to its receptor RANK on the osteoclast precursor cell surface. Downstream activation of the nuclear factor of activated T cells 1 (NFATc1) signaling causes the subsequent induction of osteoclastogenic genes (17, 18). Pro-inflammatory environments, as those found in infectious conditions, can promote osteoclastogenic differentiation of macrophages due to an inflammation-induced increase of the production of RANKL by osteoblasts (19, 20). Additionally, a direct contribution of bacterial molecules such as SA Protein A is described to promote osteoclast formation (21, 22). Increased osteoclast numbers and bone resorption play a role in the pathophysiology of implant-related bone infections, which can lead to implant loosening and loss of joint function (23, 24). It remains unclear if and how biofilm formation contributes to this process.

In order to clarify the effect of biofilm formation on macrophage immune function and osteoclastogenic differentiation, we treated RAW264.7 cells with conditioned media (CM) generated from SA or SE planktonic or biofilm cultures in the presence or absence of RANKL. We evaluated the early immune activation of the cells as well as the ability to perform osteoclast differentiation upon simultaneous stimulation with CM and RANKL. Further, we investigated potential mechanisms that could play a role in the CM-mediated effects on macrophage immune function and osteoclast differentiation.

## Results

### *CM induce an early pro-inflammatory macrophage immune response, which is less pronounced in biofilm CM*

In order to evaluate differences in early immune activation of macrophages by either planktonic or biofilm environments of SA and SE, we stimulated RAW macrophages with the respective CM for up to 24 hours. Figure 1A shows that stimulation of macrophages with staphylococcal CM increased surface protein expression of TLR-2, MHC II, CD80 and CD86. Immune activation markers were reduced in biofilm CM compared to planktonic CM. Protein levels of intracellular TLR-9 were only slightly increased with no differences between planktonic and biofilm CM. qPCR analysis revealed that CM induced gene expression of the pro-inflammatory cytokines IL-1 $\beta$ , IL-

6, TNF- $\alpha$  and IFN- $\beta$  and the anti-inflammatory cytokine IL-10. TNF- $\alpha$  and IL-10 mRNA levels were higher in biofilm CM, whereas IFN- $\beta$  mRNA levels were more induced in planktonic CM (Fig. 1B). Release of IL-1 $\alpha$ , IL-6, TNF- $\alpha$  and IL-10 was increased after CM treatment. For TNF- $\alpha$ , however, the results varied for SA or SE, as TNF- $\alpha$  was particularly high in SA biofilm and in SE planktonic CM. Interestingly, IFN- $\beta$  protein was only increased in planktonic CM with the highest amount detectable in SA planktonic CM (Fig. 1C). In line with these findings, all CM induced the NF- $\kappa$ B pathway, as indicated by increased levels of phosphorylated p65. The IRF-3 pathway responsible for IFN- $\beta$  production was only activated in SA planktonic CM (Fig. 1D). As IRF-3 can be activated in a STING (stimulator of interferon genes)-dependent manner downstream of cytosolic DNA recognition (25), we evaluated free bacterial DNA content in the CM. This reflected the contrasting results for SA and SE and showed the lowest DNA amount in SA planktonic CM (Fig. 1E). Free bacterial DNA, however, did not correlate with IFN- $\beta$  production. Further, STING-mediated IRF-3 activation can be induced by self-DNA release into the cytoplasm upon cell stress via cyclic GMP-AMP synthase (cGAS) (26). As a marker for oxidative stress, we analyzed production of reactive oxygen species (ROS) by macrophages upon stimulation with the CM, but we detected only a slight increase in ROS levels after two hours of stimulation with CM (Fig. 1F). Phagocytosis was enhanced by all CM with the highest bead uptake in SA biofilm CM. In SE, phagocytotic activity reproducibly was slightly lower in biofilm CM compared to planktonic CM (Fig. 1E). Our data suggest that planktonic as well as biofilm CM lead to a pro-inflammatory macrophage immune response, although immune surface markers were less induced in biofilm CM and IFN- $\beta$  release was only present in planktonic CM. Another interesting finding is the observed difference in planktonic versus biofilm patterns between SA and SE.

*Early macrophage immune response is dominated by glycolytic metabolism with a shift towards increased mitochondrial activity in SE biofilm CM*

As metabolism is closely linked to immune polarization, we analyzed the metabolic activity of RAW macrophages upon CM treatment. In contrast to planktonic CM, biofilm CM contained high amounts of bacterial L-lactate (Fig. 2A). L-lactate secretion by macrophages was found to be more pronounced in the presence of planktonic CM (Fig. 2B). The expression of lactate dehydrogenase A (LDHA, phosphorylated form) and monocarboxylate-transporter 1 (MCT-1), which is involved in lactate uptake, was not affected on mRNA (Fig. 2C) and protein (Fig. 2D) levels. In order to investigate glycolytic activity versus mitochondrial respiration, we analyzed the respective marker proteins eIF4E binding protein (4E-BP1) and AMP-activated protein kinase (AMPK). When 4E-BP1 is phosphorylated (inactivated) by mTORC1 (mechanistic target of rapamycin complex 1), eIF4E (eukaryotic translation initiation factor 4E) is released and can start mRNA translation of glycolytic proteins (27). As shown in Figure 2E, all CM treatment conditions increased phospho-4E-BP1 levels, which indicates an increase in signaling pathways that are involved in glycolysis during early macrophage immune response. AMPK acts as a master regulator of cellular energy homeostasis by sensing the AMP/ATP ratio within the cell. In its

phosphorylated state, AMPK blocks mTORC1 and induces ATP-producing pathways such as mitochondrial respiration (28). Figure 2E shows that phospho-AMPK levels were not as strongly affected as phospho-4E-BP1 levels during the early immune response of macrophages induced by CM. Aconitate decarboxylase 1 (ACOD-1, also known as IRG-1) catalyzes the reaction of cis-aconitate into the anti-inflammatory itaconate and regulates glycolysis-induced inflammation (29, 30). ACOD-1 gene expression was strongly induced in CM-treated macrophages (Fig. 2F). After 24 hours, ROS production was increased by all CM indicating increased immune activity and cell stress (Fig. 2G). Both, glycolysis and mitochondrial activity were induced after stimulation with CM. The strongest mitochondrial activity was detectable in SE biofilm CM (Fig. 2H). Still, total ATP levels were lower in CM-treated macrophages compared to the untreated control (Fig. 2I). This indicates that early macrophage metabolism mainly relies on aerobic glycolysis, which is associated with a pro-inflammatory immune response. Lactate release by macrophages was reduced in biofilm CM compared to planktonic CM. When biofilm CM of SE were used, macrophages shifted towards more mitochondrial activity, which in general is associated with a more anti-inflammatory immune response. If the detected higher mitochondrial polarization contributed to the energy pool of the cell by increased OxPhos or gain a more biosynthetic importance in the macrophage response was not finally clarified.

*CM suppress RANKL-induced osteoclastogenesis and favor macrophage MGC formation, which is associated with increased TNF- $\alpha$  and IL-10 levels*

Next, we investigated the ability of RAW macrophages to perform osteoclastogenic differentiation when the cells were cultured for up to 5 days in the presence of RANKL and the different CM. As expected, stimulation of macrophages with RANKL induced osteoclastogenesis, while the combined treatment with RANKL and CM severely inhibited osteoclast formation (Fig. 3A). The few osteoclasts that developed despite CM treatment were smaller and rather isolated compared to osteoclast clusters formed with RANKL alone (Fig. 3B). Total NFATc1 still was present on protein level (Fig. 3C), however, impaired osteoclastogenesis was reflected by the absence of increased NFATc1 mRNA levels in the RANKL + CM treated macrophages (Fig. 3D). This was in line with a reduced induction of the osteoclast marker genes for TRAP and ATP6Vod2 (Fig. 3E+F). Our data indicate that CM either led to a non-activating posttranslational modification of NFATc1 or interfered with downstream NFAT signaling, which resulted in diminished osteoclastogenic differentiation of RANKL + CM treated macrophages.

Evaluation of OCs showed that multinucleated giant cells (MGCs) were generated through macrophage fusion upon treatment with CM + RANKL. The MGC formation was highest in SE planktonic CM (Fig. 4A). Small MGCs also formed spontaneously in the control group (medium), but CM led to formation of large MGCs with multiple nuclei localized in the center of the cell. Further, MGCs contained granules in their cytosol and the cells showed an activated morphology with filopodia (Fig. 4B). Formation of MGCs is associated with the activation of the

IL-4/phospho-Stat6 pathway (31, 32). Figure 4C shows that CM stimulation did not lead to Stat6 activation but caused Stat3 tyrosine phosphorylation. PhosphoTyr-Stat3 levels were higher in planktonic CM compared to biofilm CM of both, SA and SE (Fig. 4C). Stat3 pathway activation is involved in an anti-inflammatory counteraction and termination of immune reaction via IL-10 but also IFN- $\beta$  (33, 34). Thus, we analyzed late cytokine production by macrophages upon CM + RANKL treatment. As shown in Figure 4D, we did not observe an induction of the IL-4 gene by CM, which correlates with the absence of Stat6 activation. Gene expression analysis of other cytokines showed that IL-1 $\beta$ , IL-6, TNF- $\alpha$  and IL-10 mRNA levels remained high at the later time point independent of RANKL presence. For SE, IL-10 mRNA levels were higher in planktonic CM compared to the biofilm CM. Release of IL-1 $\alpha$ , IL-6, TNF- $\alpha$  and IL-10 were also still increased by CM-treated macrophages despite stimulation with RANKL. Again, TNF- $\alpha$  levels were higher in SA biofilm compared to the planktonic CM and SE planktonic CM compared to the respective biofilm CM. SE planktonic CM led to the highest TNF- $\alpha$  release. Interestingly, IL-10 showed a comparable pattern with higher protein levels in SA biofilm and SE planktonic CM, respectively. Even at late time points, IFN- $\beta$  was increased in SA planktonic CM (Fig. 4E). As a marker for pro-inflammatory M1 macrophage polarization, we further analyzed NO production. iNOS gene expression was induced by RANKL and the increase was more pronounced in the presence of CM. Planktonic CM showed slightly higher iNOS mRNA levels than biofilm CM (Fig. 4F). NO release was only induced when cells were additionally treated with CM, but not with RANKL alone (Fig. 4G).

In summary, stimulation of macrophages suppresses RANKL-mediated osteoclastogenesis while inducing a long-term immune activation associated with MGC formation. This effect was most pronounced in planktonic CM of SE.

*Late macrophage immune metabolism shifts towards more mitochondrial contribution, while OxPhos complexes are reduced by CM*

We further analyzed cellular metabolic activity upon long-term treatment with CM and RANKL. Stimulation of macrophages with RANKL increased the relative mitochondrial copy number of macrophages and the addition of CM resulted in enhanced numbers compared to RANKL alone (Fig. 5A). Interestingly, RANKL did not alter mitochondrial activity, while in CM + RANKL treated cells the mitochondrial activity was highly increased (Fig. 5B). Investigation of phospho-4E-BP1 and phospho-AMPK indicated that at the later time point both, mTORC1-pathway associated glycolysis and mitochondrial ATP-production were activated by RANKL and CM + RANKL, respectively (Fig. 5C). Despite the observed increase in relative mitochondria numbers, mitochondrial activity and phospho-AMPK levels, the amount of OxPhos complexes was decreased in CM + RANKL treated macrophages, in particular, OxPhos complexes CI, CII and CIV (Fig. 5D). Our results indicate that although macrophages still exhibit a pro-inflammatory phenotype, the cells maintain glycolysis but also increase their mitochondrial biomass and

activity after long-term stimulation. This effect is most pronounced in SE biofilm CM. Since these changes in mitochondria are not accompanied by an increased expression of OxPhos complexes, it reinforces the hypothesis that the role of mitochondria is not only an energy-producing but also a biosynthetic one.

*CM effects on macrophage differentiation are rather mediated directly by bacterial molecules than by subsequent cytokine release*

In order to investigate whether CM impact on osteoclast and MGC formation are mediated directly by bacterial mediators present in the CM or rather by subsequent cytokine release of CM-treated macrophages, we stimulated RAW macrophages either with the TLR-2 ligand Pam3CSK4, the TLR-9 ligand CpG or the cytokines IL-10 and TNF- $\alpha$  in combination with RANKL (Fig. 6). TLR-2 and TLR-9 activation resulted in reduced RANKL-mediated OC formation. Induction of these two TLRs together with RANKL increased MGC numbers. However, TLR-stimulation alone was able to induce more MGCs than when combined with RANKL. IL-10 or TNF- $\alpha$  together with RANKL did not affect OC and MGC formation (Fig. 6A-C). Treatment with TLR-ligands + RANKL was accompanied by reduced NFATc1 mRNA levels, whereas cytokine stimulation did not change RANKL-mediated NFATc1 gene expression (Fig. 6D). Also, gene expression of the pro-inflammatory cytokine TNF- $\alpha$  and the anti-inflammatory cytokine IL-10 was only induced in TLR-ligand + RANKL but not in cytokine + RANKL stimulated macrophages (Fig. 6E+F). The induction of an immune response by TLR-ligands was further reflected in the activation of the Stat3 pathway, which was only present in TLR-ligand + RANKL treatment (Fig. 6G).

Our results indicate that TLR-2 and TLR-9 signaling might play a role in mediating the observed CM effects. As shown in Suppl. Figure 5, inhibition of TLR-2 and/or TLR-9 signaling indeed revealed that CM effects on macrophage immune activity and osteoclastogenesis were partially dependent on these pathways. TLR-2 signaling played a crucial role in mediating the suppressive effects on RANKL-induced NFATc1 gene expression by planktonic CM (Suppl.Fig. 5C). Regarding the induction of TNF- $\alpha$  and IL-10 gene expression by CM, both, TLR-2 and TLR-9 activation seem to be important (Suppl.Fig. 5D+E). Here, inhibition of TLR-2 signaling was more effective for CM of SA. Inhibition of TLR-9 signaling had a pronounced effect on SA biofilm and SE planktonic CM, but did not seem to play a role in macrophage response towards biofilm CM of SE.

Since IFN- $\beta$  may have a suppressive and regulatory effect on osteoclast formation (35, 36), we investigated whether IFN- $\beta$  production by macrophages stimulated with planktonic CM could be another mediator of the inhibitory effect on osteoclastogenesis. RAW macrophages were cultured in the presence of RANKL and different IFN- $\beta$  concentrations. As shown in Figure 7A+B, addition of IFN- $\beta$  resulted in a dose-dependent reduction of osteoclast formation and a slightly reduced induction of osteoclastogenic marker gene expression, whereas mRNA levels of the



down-stream target of IFN- $\beta$  signaling interferon-stimulated gene 15 (ISG-15) increased (Fig. 7C). The IFN- $\beta$  effect on osteoclast formation seemed to be dependent on an inhibition of cell proliferation as shown in Figure 7D. Stat1 pathway activation by IFN- $\beta$  became detectable at a concentration of 1 ng/ml (Fig. 7E). Thus, IFN- $\beta$  amounts secreted by macrophages in planktonic CM (median: 160.1 pg/ml, min: 134.9, max: 279.1 for SA) can partially explain the suppressive effect on osteoclastogenesis.

In summary, our data revealed that effects of planktonic CM mainly rely on TLR signaling and IFN- $\beta$  production, while these mechanisms seem to play only a minor role in biofilm CM.

#### *High lactate concentration contributes to the suppressive effects of biofilm CM on osteoclastogenic differentiation of macrophages*

We showed that biofilm CM contain high amounts of bacterial (L-) lactate. As this might contribute to the suppressive effect of biofilm CM on osteoclastogenesis, we investigated if high extracellular lactate concentrations have an effect on the osteoclastogenic differentiation capacity of macrophages. RAW macrophages were stimulated with RANKL and sodium L-lactate was added at different concentrations. Increasing L-lactate concentrations led to a decrease in the size and numbers of osteoclasts (Fig. 8A+B). mRNA levels of the transcription factor NFATc1 were only slightly reduced even at high L-lactate concentrations, whereas the expression of the NFATc1 target genes for TRAP and ATP6Vod2 was reduced in a dose-dependent manner (Fig. 8C). We further found a decrease in levels of mTORC1 target phospho-4E-BP1 at high L-lactate concentrations (15 and 20 mM). Phospho-AMPK remained unchanged. This might indicate less glycolytic activity of cells cultured under high L-lactate concentrations. However, it seemed that at 20 mM L-lactate (without RANKL) overall protein levels, including phospho-AMPK, were decreased (Fig. 8D). Staphylococci can produce L- and D-lactate and thus, lactate content within the biofilm CM most likely consists of both stereoisomers. We therefore tested if D-lactate had similar effects on macrophage osteoclastogenesis. Indeed, extracellular D-lactate led to a reduced osteoclastogenesis according to reduced RANKL-mediated induction of osteoclastogenic marker genes for TRAP and ATP6Vod2, but again NFATc1 mRNA levels remained unaffected (Fig. 8E). Thus, our data demonstrate that high lactate content of the biofilm CM plays a role in suppressing macrophage osteoclastogenesis.

## **Discussion**

Biofilm formation is a major cause for chronic progression of implant-related bone infections. Such infections are characterized by inflammation and osteoclast-mediated bone destruction, which ultimately lead to implant loosening and loss of limb function. The biofilm environment is therefore discussed to shift the immune reaction towards a more tolerogenic response that

supports bacterial persistence. Macrophages play an important role in the early defense against invading bacteria, but additionally serve as precursors for osteoclasts, thus linking inflammation and bone destruction. The aim of our study was to clarify if biofilm formation affects macrophage function regarding activity and osteoclastogenic differentiation. Therefore, we cultivated RAW264.7 cells either with or without RANKL in planktonic or biofilm CM generated from respective SA and SE cultures and analyzed immune activation, metabolic activity and osteoclast formation. Furthermore, we investigated potential mechanisms behind the CM effects. We show that both environments, planktonic and biofilm, elicit a pro-inflammatory immune response with increased glycolytic activity. However, this was less pronounced in biofilm CM. Our data further indicate that a planktonic environment initiates a strong IFN- $\beta$  response, which was not detected in the respective biofilm environment. Furthermore, both environments suppress the osteoclastogenic differentiation and induce MGC formation of macrophages. In planktonic CM, this is mainly caused by activation of TLR and IFN- $\beta$  signaling, while in biofilm CM high lactate levels are in part responsible for the observed effects.

In our study, we directly compared the effects of planktonic and biofilm environments on the macrophage immune response. Furthermore, we included two relevant bacteria strains, *Staphylococcus aureus* and *epidermidis*, and found remarkable differences between SA and SE. SA are highly virulent, produce a panel of toxins, are able to survive intracellularly and can form biofilms (9). In contrast, pathogenicity of SE mainly depends on biofilm formation (10). To address this difference, we used the SE reference strain RP62A, which possesses a high *in vitro* biofilm formation capacity (37) and the SA strain UAMS-1, which originates from an osteomyelitis patient and only shows poor biofilm formation on uncoated plastic surfaces (38, 39). Thus, the observed contrasting results between SA and SE might have been partially caused by an increased release of bacteria and EPS molecules from the rather fragile SA biofilm into the environment. In line with previous data from SA biofilm infection models (40, 41), biofilm CM of SA and SE induced less TLR-2 activation compared to planktonic CM. In planktonic and biofilm CM, TLR-9 was only slightly and comparably up-regulated. However, the inhibition of the respective TLR signaling indicated that the induction of cytokine gene expression was dependent on TLR-2 and -9 activation in both, planktonic and biofilm CM, but to a varying extent, which was weakest in biofilm CM of SE. In our approach, planktonic as well as biofilm CM of both strains induced an increased production of pro-inflammatory (IL-1, IL-6, TNF- $\alpha$ ) as well as anti-inflammatory (IL-10) cytokines by macrophages. This is in contrast to a similar study that showed a suppression of pro-inflammatory macrophage activity by biofilm CM of SA through KLF2-mediated negative regulation of NF- $\kappa$ B activation (42). The authors suggested that this increased KLF2 expression might be caused by exotoxins such as  $\alpha$ -hemolysin secreted from the biofilm. Interestingly, the UAMS-1 strain used in our study is negative for  $\alpha$ -hemolysin due to a mutation of the *hla* gene (43), which might explain the different results. In our study, the biofilm CM of SA and SE contained high amounts of bacterial lactate. In general, extracellular

lactate is associated with an inhibitory effect on the pro-inflammatory immune response of macrophages (44-46). In a recent study, the group of Tammy Kielian compared the effects of biofilm environments from wild-type and a mutant SA strain deficient in the production of L- and D-lactate on IL-10 induction (47). They found that biofilm-derived lactate is responsible for an increased IL-10 synthesis by MDSCs and macrophages via inhibition of histone deacetylase 11 (HDAC11) and unchecked *IL10* promoter activity. In our experimental setup, we detected a strong IL-10 induction by both, planktonic and biofilm CM. As we did not detect elevated levels of bacterial lactate in planktonic CM, we suggest that the mechanisms behind the increased IL-10 induction may differ between planktonic and biofilm environments. We further detected a strong IFN- $\beta$  response against planktonic CM, especially for SA. This has been described previously in a planktonic infection model (48), but we are the first to compare IFN- $\beta$  production between planktonic and biofilm CM. By this, we were able to show that, in contrast to the planktonic environment, an IFN- $\beta$  response was not triggered by the respective biofilm environment. Our results indicate that IFN- $\beta$  production may be particularly induced by post-growth planktonic bacteria to evade effective clearance by the immune system and to promote biofilm formation. Thus, inhibiting the IFN- $\beta$  response might be an attractive target to prevent planktonic to biofilm transition at the early chronic state of infection. IFN- $\beta$  production was associated with activation of IRF-3, a downstream target of STING-dependent cytosolic DNA sensors such as cGAS and DNA-dependent activator of IFN-regulatory factors (DAI) (49, 50). We could exclude bacterial dsDNA as a STING-inducing factor in our approach, as free DNA content in the CM did not correlate with IFN- $\beta$  production. Furthermore, we excluded ROS production and oxidative stress, which can result in release of mitochondrial and nuclear DNA into the cytoplasm and subsequent cGAS-mediated STING activation (26, 51). Further mechanisms that trigger IFN- $\beta$  production can be the uptake of extracellular self-DNA released upon cell death and subsequent cGAS-mediated STING activation, activation of STING by bacterial cyclic dinucleotides (CDNs) secreted into the environment (52, 53) and the induction of a TLR-dependent IFN- $\beta$  response by SA virulence factors such as protein A (54). Additional studies are necessary to determine if c-di-AMP release contributes to the differential levels of IFN- $\beta$  production or if additional mediators are involved.

We also addressed the effects of a planktonic or biofilm environment on the osteoclastogenic differentiation capacity of macrophages and added RANKL to our CM to mimic the inflammatory and osteoclastogenic environment of infected bone. Treatment of the cells with CM resulted in suppression of RANKL-induced osteoclastogenesis. NFATc1 was still present on the protein level, indicating that CM did not interrupt RANK activation, but rather interfered with downstream signaling and did not induce NFATc1-mediated osteoclastogenic gene expression. This is in line with a study which showed that LTA suppressed RANKL-mediated osteoclastogenesis through TLR-2 activation and inhibition of the DNA-binding activity of AP-1 but not NFATc1 (55). Addition of TLR-ligands or bacterial supernatants after pre-priming of macrophages with RANKL

accelerates osteoclastogenesis (56-58) through increased production of pro-inflammatory cytokines such as TNF- $\alpha$  (59, 60). Simultaneous activation of TLRs together with RANK, like in our approach, was shown to inhibit osteoclast formation of macrophages (61, 62). Thus, immune activation of macrophages has a superior role over osteoclast formation (63). Indeed, TLR-2 but not TLR-9 signaling was important for the suppression of RANKL-induced osteoclastogenic gene expression by planktonic CM in our model. TLR activation seemed not to be responsible for the anti-osteoclastogenic effect of biofilm CM. Furthermore, IFN- $\beta$  led to a dose-dependent reduction in OC formation as already mentioned in the literature (35, 64). Thus, the combined activation of TLR- and IFN- $\beta$  signaling may be the reason for the strong anti-osteoclastogenic effects of planktonic CM. The suppressive effects on osteoclastogenesis by biofilm CM were instead mediated through high amounts of bacterial lactate. Interestingly, a recent study showed that glycolysis-derived lactate produced by macrophages during osteoclastogenic activation supported bone resorption, but addition of extracellular lactate had no effect (65). This indicates that like for TLR stimulation, the effects of lactate might depend on the commitment stage of macrophages but also on the source and concentration of the lactate. So far, our data indicate that neither planktonic nor biofilm CM directly support RANKL-induced osteoclast formation *in vitro*. Long-term exposure of macrophages to CM and RANKL instead resulted in the formation of MGCs, which are generally associated with chronic inflammation. Physiologically, this can be observed in granuloma formation and foreign body reactions. The exact function of MGCs is still unclear and seems to depend on the disease context (66, 67). MGCs are also found in dental implant infections (67), but to our knowledge, a contribution of MGCs in the context of staphylococci planktonic and biofilm environments has not been described so far. We found MGC formation upon CM treatment to be independent of the IL-4/Stat6 pathway, which was described for the generation of foreign body giant cells (FBGCs) (32, 68). Instead, we detected activation of the Stat3 pathway that is involved in termination of inflammation when it is induced by IL-10 and IFN- $\beta$  (33, 34). Phospho-Stat3 levels were higher in planktonic compared to biofilm CM indicating the onset of resolution processes of the early pro-inflammatory macrophage response, which was initially more pronounced in planktonic CM. High IFN- $\beta$  levels might have also contributed to increased Stat3 pathway activation in planktonic CM. As MGC numbers did not correlate with phospho-Stat3 levels, Stat3 pathway activation seems not to be responsible for MGC formation. Still, TNF- $\alpha$  and IL-10 were positively associated with MGC numbers, which indicates that these cytokines can contribute to MGC formation and function, respectively. Interestingly, effects on MGC formation and cytokine secretion were strongest in planktonic CM of SE. In contrast to SA, SE only possesses a few virulence factors, including Phenol-soluble modulins (PSMs). PSMs belong to a class of secreted peptides of which some have cytolytic activity (10) and are involved in biofilm structuring and dispersal (69). Further, PSMs can be recognized by innate immune cells either directly through interaction with formyl peptide receptor 2 (FPR2) (70) or indirectly by increased release of lipopeptides that lead to TLR-2 activation (71). A possible role of PSMs in the differential

macrophage immune responses towards staphylococci planktonic and biofilm CM and in MGC formation has to be clarified in future studies.

The pro-inflammatory immune response was characterized by increased glycolysis. For SE biofilm CM, however, an increased mitochondrial activity was detectable already at the early time point, which is associated with a more anti-inflammatory M2 macrophage polarization (72). This is in line with another study, which showed a shift towards OxPhos in monocytes over the time course of an orthopedic biofilm infection. Furthermore, the authors showed that inhibiting OxPhos *in vivo* restored an effective monocyte immune response and reduced biofilm burden (73). In our approach, late macrophage phenotype showed a shift towards increased mitochondrial biomass and activity. RANKL-mediated osteoclastogenesis is relying on both glycolysis and OxPhos (74), which is in line with our findings that both, mTORC1-dependent glycolysis (indicated by increased level of phospho-4EB-P1) and relative mitochondria numbers are up-regulated in the RANKL control. Another study showed a pre-dominant role of glycolysis during osteoclastogenesis and an inhibitory effect of activated AMPK, but also argued with the importance of maintaining ATP levels during this energy consuming differentiation process (75). Interestingly, mitochondrial activity was not changed by cells treated with RANKL only. Addition of CM, however, strongly increased mitochondrial activity, which was more pronounced in biofilm compared to planktonic CM. A recent paper showed that IL-10 is important for preventing accumulation of dysfunctional mitochondria and associated ROS production upon a bacterial stimulus. This effect was mediated through increased induction of mitophagy via inhibition of mTORC1 (76). Increased IL-10 levels upon CM treatment of macrophages might support mitochondrial functionality after additional stimulation with RANKL. In addition, NO production, a main characteristic for M1 macrophage polarization, was increased. This is discussed to reduce OxPhos activity and to prevent M2 re-polarization into pro-inflammatory M1 macrophages (77). In our model, OxPhos proteins (CI, CII and CIV) were decreased in CM-treated macrophages, which was also shown for long-term LPS stimulated cells (72 hours) and was associated with glycolysis and pro-inflammation (78). Our data argue for a heterogenous late macrophage response, which seems to be pre-dominantly pro-inflammatory, but already shifted towards an increased mitochondrial contribution that is in general associated with an anti-inflammatory state. This tendency was more pronounced in the biofilm environment. The observed changes could be the result of a feedback loop in which the initial pro-inflammatory reaction induces a subsequent anti-inflammatory counteraction via IL-10/Stat3 signaling to avoid long-term inflammation and tissue damage. Furthermore, a shift from glycolysis to mitochondrial respiration is required to restore energy sources, which were used up by the initial pro-inflammatory reaction. If indeed, increased mitochondrial biomass and activity pre-dominantly contributed to energy production via mitochondrial respiration or were more recruited for biosynthetic purposes has yet to be resolved. The here detected reduction of ATP levels and OxPhos proteins after CM treatment argues for a dual function of mitochondria. At

this point it further remains unclear whether the metabolic profile of the biofilm environment with low glucose and high lactate levels is the driver of this phenotypical change during an ongoing macrophage immune response and needs further investigation. Overall, we suggest that bacterial lactate that is highly enriched within the local biofilm microenvironment as well as concomitant deprivation of glucose may impair energy-consuming and biosynthetically costly processes such as long-term inflammation and osteoclast formation of macrophages, respectively.

There are some limitations of our study: we used the murine macrophage cell line RAW264.7, which was established from an Abelson murine leukemia virus-induced tumor. Thus, we cannot exclude that some results, especially the metabolic aspects, might have been affected by the cancer nature of the cells. Therefore, the key results of our study such as the different induction of an IFN- $\beta$  response should be repeated in primary cells. Furthermore, conditioned media allowed us to perform *in vitro* osteoclastogenesis experiments, but the direct interaction of bacteria / biofilms and macrophages are omitted in such an indirect experimental setup. In order to investigate the impact of the biofilm itself, the use of heat-inactivated biofilms might be a possible approach.

In conclusion, our study showed that staphylococci planktonic and biofilm environments differentially interfere with macrophage function. Both conditions lead to immune activation of macrophages and suppression of RANKL-induced osteoclastogenic differentiation. However, the underlying mechanisms differed. While the effects of a planktonic environment on macrophage differentiation mainly depend on activation of TLR- and IFN- $\beta$  signaling, in the biofilm environment high lactate levels are additionally involved in the inhibition of osteoclastogenesis. These distinct scenarios have to be considered regarding therapeutic intervention. Modulation of the IFN- $\beta$  response may be a possible approach for preventing planktonic to biofilm transition. Targeting the effect of bacterial lactate could be a promising strategy to strengthen the immune response against mature biofilms. Thus, our data can help to develop individual treatment options to either prevent or treat biofilm formation in implant-related bone infections.

## Materials and Methods

### Study design

With this study, we wanted to investigate the early immune response of macrophages to either a planktonic or biofilm environment, respectively (Suppl. Fig. 1). Therefore, cells were cultivated in conditioned media (CM) of planktonic or biofilm cultures of SA or SE 1:1 diluted in fresh growth media for up to 24 hours. Post-hoc, surface marker profile (FACS), cytokine expression

(qPCR, CBA), signal transduction (WB) and immune metabolism (glycolysis vs. TCA/OxPhos) were analyzed (Suppl. Table 1). Further, we wanted to investigate the impact of SA / SE planktonic or biofilm environment on receptor activator of NF- $\kappa$ B ligand (RANKL)-induced osteoclastogenic differentiation of macrophages. Therefore, macrophages were stimulated with 1:1 diluted CM and RANKL in parallel for up to 5/6 days and osteoclast (OC) formation was evaluated by gene expression analysis of osteoclastogenic markers and tartrate-resistant acid phosphatase (TRAP) staining. Additionally, late immune response was analyzed as described for the first part (Suppl. Table 1). As bacteria used up most nutrients within the media, we diluted the CM 1:1 in fresh growth media to allow cell survival and differentiation for up to 6 days. To evaluate if the impact of CM on RANKL-induced osteoclastogenesis was directly based on bacterial molecules secreted in the media or was induced by cytokines produced by the macrophages themselves as response to CM, cells were stimulated with relevant TLR-ligands, L- or D-lactate or cytokines, respectively, and gene expression, signal transduction and OC / MGC formation were determined (Suppl. Table 1).

#### Bacteria culture and preparation of conditioned media

*Staphylococcus aureus* strain ATCC 49230 (USA200, UAMS-1, isolated from a patient with chronic osteomyelitis (39)) and *Staphylococcus epidermidis* strain DSM 28319 (ATCC 35984, RP62A, isolated from a catheter sepsis) were used for preparation of conditioned media. As already described in the literature, SA strain ATCC 49230 is a weak biofilm producer under standard *in vitro* conditions (38), whereas SE strain DSM 28319 is known to possess a strong *in vitro* biofilm formation capacity on plastic (37) (Suppl. Fig. 2A). Bacteria were cultured on Columbia agar plates with 5% sheep blood (BD, Germany) and streaked onto fresh agar plates a day before experiment. 3 to 5 colonies were transferred into trypticase soy bouillon (TSB; BD, Germany) and cultivated under shaking for 3 hours at 37 °C to receive growth state bacteria. Bacteria concentration was measured photometrically (Den-1, Grant Instruments, UK) and adjusted to a concentration of  $6 \times 10^5$  CFU/ml in DMEM high glucose (Anprotec, Germany) + 10% fetal calf serum (FCS; Thermo Fisher Scientific, USA). For planktonic culture, bacteria were cultivated under shaking (200 rpm) for 24 hours at 37°C and 5% CO<sub>2</sub>. For biofilm culture, bacteria were plated in 24 well with 1 ml per well and cultivated under static conditions for 3 or 6 days (Suppl. Fig. 2B). In biofilm cultures, medium was replaced every 24 hours. For CM, planktonic medium after 24 hours of culture or the last 24 hours medium change before day 3 or 6 biofilm culture was harvested by centrifugation at 4000 rpm for 15 min at 4°C. For biofilm CM, media of wells from one plate were pooled before centrifugation. Harvested media were streaked onto agar plates, cultivated over night at 37°C and bacterial appearance (colony size and color) was controlled to ensure no contamination by other bacteria. Supernatants were then sterile filtered through a 0.2  $\mu$ m filter and frozen at -80°C (Suppl. Fig. 2C). To rule out remaining bacterial growth, sterile filtered media were inoculated in TSB and cultivated over night at 37°C. Before use in cell culture, pH of CM was adjusted to pH of growth medium

(DMEM high glucose + 10% FCS), 1% Penicillin / Streptomycin (Pen/Strep; Anprotec, Germany) was added and aliquots were stored at -80°C. Planktonic and biofilm CM from the same approach were compared within one experiment. For unstimulated CM control, growth medium (DMEM high glucose + 10% FCS) of the respective approach was treated analogously to CM without bacteria inoculation. Within this study six independent batches of CM were included. One representative CM approach was evaluated for metabolites in <sup>1</sup>H NMR (Suppl. Fig. 2D). Spectra of the different CM showed that glucose was degraded with small amounts left only in planktonic CM. Bacteria produced acetate in planktonic as well as biofilm conditions, whereas lactate was only released in the media of biofilm cultures.

#### Free bacterial DNA content in CM

DNA was extracted from 1 ml of three representative CM approaches, respectively, using the DNeasy® Blood and Tissue Kit from Qiagen, Germany. The cell lysis step was skipped and 500 µl 100% ethanol were directly added to the sample. The following steps were done according to the manufacturer's protocol. DNA was eluted in 30 µl elution buffer and 12 µl of the DNA eluate was used for qPCR. DNA was amplified for 40 cycles using SA specific primers for gyrase B (fw: AGTAACGGATAACGGACGTGGTA, rev: CCAACACCATGTAAACCACCGAT) and SE specific primers for gyrase A (fw: AGCAGCAGGTGTGAAAGGTA, rev: TACGCTCGGTAATTGTGCGCA). PCR products were visualized by agarose gel electrophoresis.

#### Cell culture and stimulation of macrophages

The murine macrophage cell line RAW264.7 (ATCC TIB-71, USA) was used for the experiments (79). RAW264.7 cells were cultivated in DMEM high glucose + 10% FCS + 1% Pen/Strep at 37°C and 5% CO<sub>2</sub> and were split 3 times a week. Cells were used in the experiments two weeks after thawing for up to 6-8 weeks. Before experiments, cells were harvested by scraping, centrifuged at 1300 rpm for 5 min and resuspended in fresh growth media (DMEM high glucose + 10% FCS + 1% Pen/Strep) at appropriate concentration. Cells then were transferred into suitable well plate formats, treated with CM 1:1 diluted in fresh cell growth media, TLR-ligands (Pam3CSK4: 25 ng/ml and CpG ODN 1668: 25 ng/ml, both InvivoGen, USA), sodium L- or D-lactate (5, 10, 15 and 20 mM, both Sigma-Aldrich, Germany) or recombinant murine cytokines (IL-10: 25 ng/ml, Peprotech, USA; TNF-α: 25 ng/ml, eBioscience, Germany or IFN-β: 0.02, 0.2 and 2 ng/ml, BioLegend, USA) ± recombinant mouse RANKL (50 ng/ml, R&D systems, UK) and analyzed for immune function, signal transduction, metabolic activity and differentiation (OC / MGC formation) after respective time points. A positive control (PC) stimulated by 1 µg/ml TLR-2 ligand Pam3CSK4 and 100 nM TLR-9 ligand CpG (both InvivoGen, USA) was included in each respective experiment for investigation of CM effects on early immune function of macrophages (Suppl. Fig. 4). In experiments with incubation times longer than 2 days 50 µM β-mercapto ethanol (PAN - Biotech GmbH, Germany) was added to reduce cell proliferation and avoid



overgrowing of RAW264.7 macrophages. Furthermore, in these experiments half of medium was exchanged late at day 2 or early at day 3 and if necessary at day 5 and cells were re-stimulated with half of stimuli (Suppl. Table 2).

### Flow cytometry

For FACS analysis, 2 million cells / well were plated in 6 well format with 1 ml fresh growth media and 1 ml CM (Suppl. Table 2). After 20 hours supernatants were frozen at  $-80^{\circ}\text{C}$  for further investigation and cells were washed twice with cold PBS. Cells were then scraped in 1 ml cold PBS with 2% bovine serum albumin (BSA, Anprotec, Germany). For surface marker staining, 100  $\mu\text{l}$  of cell suspension was either left in PBS / 2% BSA for the unstained control or stained with 0.2 mg/ml FITC anti-TLR-2 (Novus Biologicals, UK), PE anti-MHC II (invitrogen, USA), PE anti-CD80 or PE anti-CD86 (both BioLegend, USA) antibodies at  $4^{\circ}\text{C}$  for 1 hour. Cells were washed two times in cold PBS, resuspended in 150  $\mu\text{l}$  cold PBS and then analyzed with the BD FACSCanto™ Flow Cytometer (BD Biosciences, USA). After measurement, unstained controls were additionally incubated with 30 nM Sytox<sup>R</sup> Green nucleic acid stain (invitrogen, USA) for 5 min and live / dead contribution was recorded. For intracellular staining of TLR-9, 500  $\mu\text{l}$  of cell suspension were combined with 500  $\mu\text{l}$  fixation buffer (BioLegend, USA), incubated at  $37^{\circ}\text{C}$  for 15 min, centrifuged at 2000 rpm for 5 min, 2x washed with PBS / 5% BSA and then stored at  $4^{\circ}\text{C}$  over night in PBS / 5% BSA. Next day, cells were centrifuged and resuspended in 1 ml of  $-20^{\circ}\text{C}$  cold TruePhos™ Perm Buffer (BioLegend, USA) and incubated at  $-20^{\circ}\text{C}$  for 1 hour. Cells were then washed two times and resuspended in 500  $\mu\text{l}$  PBS / 2% BSA. 100  $\mu\text{l}$  of cell suspension was either kept unstained, stained with 0.5 mg/ml Alexa647 anti-TLR-9 antibody (Novus Biologicals, UK) or respective isotype at RT for 30 min. Cells were washed twice, resuspended in 300  $\mu\text{l}$  PBS / 2% BSA and analyzed with the BD FACSCanto™ Flow Cytometer. All cells except of debris were included in further analysis using the Flowing Software (version 2.5.1, Turku Bioscience, Finland).

### Cytokine bead array

20 hours supernatants of FACS surface marker analysis or supernatants of 48 hours gene expression analysis were used for cytokine bead array (CBA, LegendPlex, BioLegend, USA) (Suppl. Table 2) according to the manufacturer's protocol. A Mouse Inflammation Panel (Mix and Match Subpanel) was used including IL-1 $\alpha$ , IFN-gamma, TNF- $\alpha$ , IL12p70, IL-1 $\beta$ , IL-10, IL-6 and IFN- $\beta$ . In short, supernatants were centrifuged, diluted 1:5 (20 hours) or 1:10 (48 hours) with Assay Buffer, standard samples were prepared and samples were transferred into a V-bottom plate. Bead mix was prepared, added to the samples and incubated on a shaker over night at  $4^{\circ}\text{C}$  in the dark. Next day, plate was washed 2 times and incubated with detection antibody for 1 hour at RT while shaking. SA-PE was added and further incubated for 30 min at RT while shaking. Plate was washed two times, bead pellet was resuspended in wash buffer and

data acquisition was done with the BD<sup>®</sup> LSR II Flow Cytometer. Analysis and calculation of cytokine concentrations were performed with the included LEGENDplex<sup>™</sup> Data Analysis Software (version 8.0).

#### ROS assay

ROS production as marker for cell stress was measured after 2- and 24-hours stimulation with CM 1:1 diluted with fresh growth media (Suppl. Table 2). 5  $\mu$ M of an oxidative stress reagent (stock conc.: 2.5 mM in DMSO, CellROX<sup>™</sup> Orange Reagent, invitrogen, USA) was added to the cells for 30 min at 37°C and 5% CO<sub>2</sub>. Cells were washed three times with PBS, scraped in PBS and transferred into FACS tubes. ROS production was analyzed with the BD FACSCanto<sup>™</sup> Flow Cytometer according to the fluorescence intensity of the dye. All cells except of debris were included in further analysis using the Flowing Software (version 2.5.1, Turku Bioscience, Finland).

#### Phagocytosis assay

2 million cells / well were incubated in 6 well format with 1 ml fresh growth media and 1 ml CM for 24 hours (Suppl. Table 2). Cells were scraped, transferred into 1.5 ml reaction tubes and centrifuged. 1 ml media was removed and cells were resuspended in remaining 1 ml media. 50  $\mu$ l FITC-coupled latex bead suspension (1:10 in fresh growth media; Sigma-Aldrich, Germany) was added, homogenized and cells were incubated for 1 hour at 37°C and 5% CO<sub>2</sub>. A 4°C media sample was placed into the fridge. Cells were washed three times in cold PBS and then resuspended in PBS containing 4% formaldehyde. Fixed cells were transferred into FACS tubes and analyzed with the BD FACSCanto<sup>™</sup> Flow Cytometer. All cells except of debris were included in further analysis using the Flowing Software (version 2.5.1, Turku Bioscience, Finland).

#### Gene expression analysis

For gene expression analysis of early or late macrophage response, cells were plated according to Suppl. Table 2 and stimulated either for 4 hours or 48 hours with 1:1 fresh growth media and CM or growth media with sodium L- or D-lactate / respective TLR-ligands / cytokines  $\pm$  50 ng/ml RANKL at 37°C, 5% CO<sub>2</sub>. Supernatants were removed and either discarded (4 hours) or frozen (48 hours) and cells were stored at -80°C until further processing. Total RNA extraction was performed using the innuPREP RNA Mini Kit 2.0 (analytik jena, Germany) according to the manufacturer's protocol. In short, cells were scraped in lysis buffer and transferred to a DNA elution column. RNA in the lysate was precipitated by adding 70% ethanol, transferred to an RNA column, washed and eluted in H<sub>2</sub>O. Total RNA concentration was measured using the NanoDrop<sup>®</sup> ND-1000 spectrophotometer (Thermo Scientific, Germany). 1  $\mu$ g of total RNA was subjected to cDNA synthesis using the Biozym cDNA synthesis Kit (Biozym Scientific GmbH, Germany) according to the manufacturer's protocol using Oligo (dT) primer. A noRT sample

(w/o Reverse Transcriptase) consisting of pooled total RNA of all samples of one experiment was prepared. cDNA was diluted 1:1 in H<sub>2</sub>O and stored at -20°C. 2 µl cDNA template and 400 nM of respective primer pairs (Table 1) were used in qPCR. mRNA levels were evaluated in a two-step PCR reaction (StepOnePlus Real-Time PCR Cycler, Applied Biosystems, USA) with 60°C annealing/extension temperature for 40 cycles using the 2x qPCR BIO SyGreen Mix Hi-ROX (PCR Biosystems Ltd., UK). Quality of qPCR runs and specificity of qPCR products were controlled by included noRT and water samples for each experiment and primer pair and melting curve comparison. mRNA levels of the respective genes of interest (Table 1) were normalized to the reference gene HPRT-1 and calculated by the 2<sup>-ΔCT</sup> method.

### Immunoblotting

For protein analysis by Western Blot, cells were plated as stated in Suppl. Table 2 and stimulated with CM 1:1 diluted in fresh growth media or growth media with sodium L-lactate / respective TLR-ligands / cytokines ± 50 ng/ml RANKL for the respective time points. Supernatants were removed, cells were washed once with PBS and stored at -80°C until further processing. Cells were lysed in RIPA buffer (1% v/v NP-40 (IGEPAL® CA-630), 0.25% sodium deoxycholate, 50 mM Tris pH 8.0, 150 mM NaCl, 1 mM EDTA pH 8.0, 1 mM Na<sub>3</sub>VO<sub>4</sub>, 1 mM NaF) with EDTA-free protease inhibitors (cOmplete™ Tablets) and phosphatase inhibitors (PhosSTOP™, both Roche Diagnostics GmbH, Germany) for 1 hour at 4°C under rotation. Lysates were centrifuged at 14000 rpm for 20 min at 4°C, supernatants were transferred into fresh 1.5 ml reaction tubes and stored at -80°C. Protein concentration were determined by BCA assay (Cyanagen Srl, Italy), samples were adjusted to 10 µg protein per 20 µl with ddH<sub>2</sub>O and 5 µl 4x SDS sample buffer with 10% β-mercapto ethanol, shaken for 2 min at 95°C and stored at -20°C. 10 µg protein was loaded on pre-cast gradient 4-20% Tris-glycine gels (anamed Elektrophorese GmbH, Germany) covered with Laemmli buffer for SDS PAGE (Serva Electrophoresis GmbH, Germany) and separated at 120 V. 5 µl of broad range, color prestained protein standard (New England Biolabs GmbH, Germany) was included on each gel. Proteins were transferred onto an Amersham™ Protran™ 0.45 µm nitrocellulose membrane (GE Healthcare, UK) covered in 4+4 Whatman papers (GE Healthcare, UK) soaked in transfer buffer (192 mM glycine, 25 mM Tris, 2.6 mM SDS, 0.5 mM Na<sub>3</sub>VO<sub>4</sub>, 15% v/v methanol) for 1 hour at 2 mA/cm<sup>2</sup>. Membranes were stained with Ponceau S stain (0.5 % Ponceau S, 3 % trichloroacetic acid, 96.5 % ddH<sub>2</sub>O) for 1 min to visualize transferred proteins. Membranes then were cut according to sizes of investigated proteins to allow detection of multiple proteins. Membranes were blocked with BlueBlock PF (Serva Electrophoresis GmbH, Germany) for 30 min at RT with continuous shaking. Membranes were incubated with primary antibodies (Table 2) diluted in BlueBlock PF in 50 ml falcon tubes rolling over night at 4°C. After three times washing with TBST, membranes were incubated with the respective HRP-linked secondary antibody (Table 2) for 1 hour at RT under shaking and again washed three times. Blots were developed with ECL substrate (WESTAR ETA C ULTRA 2.0, Cyanagen Srl, Italy) and imaged in the ChemoStar ECL & Fluorescence Imager (Intas Science

Imaging Instruments GmbH, Germany). In some cases, membranes were reused after stripping with acidic stripping buffer (0.5 M 96% acetic acid, 0.5 M NaCl, pH 2.5) for 3-5 min and neutralization (20 mM Tris, pH 8.8). Stripping efficiency was tested by subsequent incubation with secondary antibody and ECL development. If no remaining bands could be detected, membranes were processed as described above beginning with the step of blocking.

#### L-lactate detection

$5 \times 10^4$  cells were plated in 96 well plates and stimulated with CM 1:1 diluted in fresh growth media for 24 hours (Suppl. Table 2). Supernatants of three replicates were pooled and stored at  $-80^\circ\text{C}$  until further processing. L-lactate concentration was measured in CM as well as in supernatants of CM stimulated macrophages using an enzyme-based bioluminescent assay according to the manufacturer's protocol (Lactate-Glo™ Assay, Promega GmbH, Germany). CM and supernatants were used 1:50 (planktonic CM) or 1:100 (other) diluted with PBS, a standard curve with defined L-lactate concentrations (0 – 200  $\mu\text{M}$ ) was included. Samples and standard were incubated with the lactate detection reagent for 1 hour at RT and light emission was recorded by luminometer (LUMIstar® Optima, BMG LABTECH, USA). L-lactate secretion by macrophages was calculated by subtracting total extracellular lactate of supernatants from lactate delivered by CM 1:1 diluted in fresh growth media.

#### ATP detection

$5 \times 10^4$  cells were plated in 96 well plates and stimulated with CM 1:1 diluted in fresh growth media for 24 hours (Suppl. Table 2). Samples were performed in triplicates. Media were removed and 100  $\mu\text{l}$  of CTG reagent (CellTiter-Glo®, Promega GmbH, Germany; 1:1 with PBS) per well was added. Cells were lysed for 1 min at RT under continuous shaking. After 10 min incubation in the dark, supernatants were transferred into a white 96 well plate. Relative ATP content was determined by bioluminescent light reaction in a luminometer.

#### Mitochondrial activity

Mitochondrial activity was measured after 24 hours and 4 days stimulation with CM 1:1 diluted with fresh growth media  $\pm$  RANKL (Suppl. Table 2). 100 nM of a mitochondrial membrane potential-sensitive dye (stock conc.: 1 mM in DMSO, MitoTracker® Deep Red FM, Cell Signaling Technology, USA) was added to the cells for 30 min at  $37^\circ\text{C}$  and 5%  $\text{CO}_2$ . Cells were washed three times with cold PBS, scraped in PBS and transferred into FACS tubes. Mitochondrial activity was analyzed with the BD FACSCanto™ Flow Cytometer according to the fluorescence intensity of the dye. Only the living cell population was included in further analysis using the Flowing Software (version 2.5.1, Turku Bioscience, Finland).

#### Mito copy No.

$1 \times 10^5$  macrophages per 24 well in 500  $\mu$ l fresh growth media were stimulated with 500  $\mu$ l CM and 50 ng/ml RANKL for 4 days. A half media exchange and re-stimulation was performed at day 2-3 (Suppl. Table 2). Media were removed and cells were stored at  $-80^\circ\text{C}$ . DNA was extracted of cells using the innuPREP DNA Mini Kit (analytik jena, Germany) according to the manufacturer's protocol. In short, cells were lysed in lysis solution containing Proteinase K and DNA was extracted by a DNA binding column. DNA concentration of the eluate was measured using the NanoDrop<sup>®</sup> ND-1000 spectrophotometer. 10 ng DNA was set in qPCR with  $60^\circ\text{C}$  annealing/extension temperature for 40 cycles. Primer pairs specific for murine nuclear DNA (nDNA: B2M fw ATGGGAAGCCGAACATACTG, B2M rev CAGTCTCAGTGGGGTGAAT, NC\_000068.8) and mitochondrial DNA (mtDNA: fw CTAGAAACCCCGAAACCAAA, rev CCAGCTATACCAAGCTCGT, NC\_005089.1) were used for amplification of specific DNA products with 2x qPCRBIO SyGreen Mix Hi-ROX. Specificity of products was controlled by water sample and melting curves. Mito copy No. was calculated according to formula: mtDNA per cell (nDNA) =  $2 \times 2^{\Delta\text{CT}}$ ,  $\Delta\text{CT} = (\text{nDNA CT} - \text{mtDNA CT})$ .

#### NO detection

$2.5 \times 10^4$  cells were plated in 96 well plates and stimulated with CM 1:1 diluted in fresh growth media + 50 ng/ml RANKL for 48 hours (Suppl. Table 2). Supernatants were directly used for NO detection in Griess Assay. 50  $\mu$ l sample as well as 50  $\mu$ l of  $\text{NaNO}_2$  standard diluted in media (100 - 2.5  $\mu\text{M}$ ) and blank were transferred into half-area 96 well plates in duplicates. 50  $\mu$ l of Griess Reagent (1:1 solution A+B, mixed before use; A: 1% sulfonamide, 5% v/v  $\text{H}_3\text{PO}_4$  in ddH<sub>2</sub>O; B: 0.1% NED in ddH<sub>2</sub>O) was added and color reaction was determined at OD 540 / 620 nm in an absorbance microplate reader (Sunrise<sup>™</sup>, Tecan Trading AG, Switzerland). NO concentrations of samples were calculated by standard curve with the Tecan's Magellan<sup>™</sup> software.

#### TRAP staining

TRAP staining of formed osteoclasts was performed after 5 or 6 days of incubation with CM 1:1 diluted in fresh growth media or growth media with sodium L-lactate / respective TLR-ligands / cytokines + 50 ng/ml RANKL. 50  $\mu\text{M}$   $\beta$ -mercapto ethanol was added to the media to avoid overgrowth by non-differentiating cells and a half media exchange and re-stimulation was performed at day 2-3 and at day 5 when a 6-day differentiation was necessary (Suppl. Table 2). Media were removed and cells were fixed with fixation solution (26% v/v citrate solution 27 mM pH 3.6, 66% v/v acetone, 8% v/v 37% formaldehyde) for 30 sec. at RT. Cells were washed with ddH<sub>2</sub>O and 400  $\mu$ l pre-warmed staining solution (1% v/v Naphthol AS-BI phosphoric acid solution, 2% v/v tartrate solution, 4% v/v acetate solution 2.5 M pH 5.2 and 2% v/v diazotated Fast Garnet solution (1:1 sodium nitrite solution and Fast Garnet GBC Base solution, prepared in advance) in ddH<sub>2</sub>O, from Acid Phosphatase Kit, Sigma-Aldrich, Germany) was added per well and incubated at  $37^\circ\text{C}$  for 30-60 min. Intensity of color reaction was checked after 30 and 45

min. Cells were washed with ddH<sub>2</sub>O and nuclei were counterstained with hematoxylin solution (Gill No. 3, Kit component) for 1 min. After removing hematoxylin solution, nuclei stain was developed with tap water for 10 min. Cells were washed with ddH<sub>2</sub>O and dried with open lid over night. Osteoclast and MGC formation were evaluated by counting of cells in 10x magnification using a cell culture microscope. Osteoclasts were defined as large TRAP positive multinucleated cells (> 3 nuclei) with plain cell borders and clear cytosol, MGCs were defined as TRAP negative multinucleated cells (> 3 nuclei) having a more diffuse cell shape including granules. Pictures were taken with the Rebel microscope (Echo, USA).

### Statistical analysis

Group sizes, data presentation and statistical test used for respective experiments are stated in the corresponding figure legends. Calculated p-values are included in the figures. As the main purpose of the study was to evaluate differences between planktonic and biofilm environments, statistical comparisons were done between SA planktonic and biofilm CM ± RANKL or SE planktonic and biofilm CM ± RANKL, respectively, using the non-parametric Mann-Whitney U (MWU) test. Thus, there were no statistical comparisons performed between medium or RANKL control and respective CM-treated samples to avoid multiple testing. Furthermore, statistical differences were analyzed between medium and positive control (PC) or medium and RANKL control to ensure quality of the experiments. For statistical comparison of more than two groups the non-parametric Kruskal-Wallis test was conducted. Experiments with only 3 replicates were not statistically evaluated. Data analysis was performed with GraphPad Prism for Windows (Version 5, GraphPad Software Inc., USA).

### Acknowledgements

Elisabeth Seebach was funded by the Physician Scientist Program of the Medical Faculty of Heidelberg University. We would like to thank Katharina Draxel, Paulina Schad and Stella Cavicchioli for their help with the experiments. We also thank Judith Schenz (Department of Anesthesiology, Heidelberg University Hospital) for critical discussion of the data. Furthermore, we thank Gabriele Sonnenmoser for technical assistance.

### References

1. Zimmerli W, Sendi P. 2017. Orthopaedic biofilm infections. *APMIS* 125:353-364.
2. Tande AJ, Patel R. 2014. Prosthetic joint infection. *Clin Microbiol Rev* 27:302-345.
3. Otto M. 2018. Staphylococcal Biofilms. *Microbiol Spectr* 6:
4. Watters C, Fleming D, Bishop D, Rumbaugh KP. 2016. Host Responses to Biofilm. *Prog Mol Biol Transl Sci* 142:193-239.

5. Zimmerli W, Sendi P. 2011. Pathogenesis of implant-associated infection: the role of the host. *Semin Immunopathol* 33:295-306.
6. Arciola CR, Campoccia D, Montanaro L. 2018. Implant infections: adhesion, biofilm formation and immune evasion. *Nat Rev Microbiol* 16:397-409.
7. Seebach E, Kubatzky KF. 2019. Chronic Implant-Related Bone Infections-Can Immune Modulation be a Therapeutic Strategy? *Front Immunol* 10:1724.
8. Gries CM, Kielian T. 2017. Staphylococcal Biofilms and Immune Polarization During Prosthetic Joint Infection. *J Am Acad Orthop Surg* 25 Suppl 1:S20-S24.
9. Muthukrishnan G, Masters EA, Daiss JL, Schwarz EM. 2019. Mechanisms of Immune Evasion and Bone Tissue Colonization That Make Staphylococcus aureus the Primary Pathogen in Osteomyelitis. *Curr Osteoporos Rep* 17:395-404.
10. Le KY, Park MD, Otto M. 2018. Immune Evasion Mechanisms of Staphylococcus epidermidis Biofilm Infection. *Front Microbiol* 9:359.
11. Masters EA, Trombetta RP, de Mesy Bentley KL, Boyce BF, Gill AL, Gill SR, Nishitani K, Ishikawa M, Morita Y, Ito H, Bello-Irizarry SN, Ninomiya M, Brodell JD, Jr., Lee CC, Hao SP, Oh I, Xie C, Awad HA, Daiss JL, Owen JR, Kates SL, Schwarz EM, Muthukrishnan G. 2019. Evolving concepts in bone infection: redefining "biofilm", "acute vs. chronic osteomyelitis", "the immune proteome" and "local antibiotic therapy". *Bone Res* 7:20.
12. Murray PJ, Wynn TA. 2011. Protective and pathogenic functions of macrophage subsets. *Nat Rev Immunol* 11:723-737.
13. Sica A, Mantovani A. 2012. Macrophage plasticity and polarization: in vivo veritas. *J Clin Invest* 122:787-795.
14. Benoit M, Desnues B, Mege JL. 2008. Macrophage polarization in bacterial infections. *J Immunol* 181:3733-3739.
15. Van den Bossche J, O'Neill LA, Menon D. 2017. Macrophage Immunometabolism: Where Are We (Going)? *Trends Immunol* 38:395-406.
16. Yamada KJ, Kielian T. 2019. Biofilm-Leukocyte Cross-Talk: Impact on Immune Polarization and Immunometabolism. *J Innate Immun* 11:280-288.
17. Kubatzky KF, Uhle F, Eigenbrod T. 2018. From macrophage to osteoclast - How metabolism determines function and activity. *Cytokine* 112:102-115.
18. Xing L, Schwarz EM, Boyce BF. 2005. Osteoclast precursors, RANKL/RANK, and immunology. *Immunol Rev* 208:19-29.
19. Josse J, Velard F, Gangloff SC. 2015. Staphylococcus aureus vs. Osteoblast: Relationship and Consequences in Osteomyelitis. *Front Cell Infect Microbiol* 5:85.
20. Souza PP, Lerner UH. 2013. The role of cytokines in inflammatory bone loss. *Immunol Invest* 42:555-622.
21. Mendoza Bertelli A, Delpino MV, Lattar S, Giai C, Llana MN, Sanjuan N, Cassat JE, Sordelli D, Gomez MI. 2016. Staphylococcus aureus protein A enhances osteoclastogenesis via TNFR1 and EGFR signaling. *Biochim Biophys Acta* 1862:1975-1983.
22. Wang Y, Liu X, Dou C, Cao Z, Liu C, Dong S, Fei J. 2017. Staphylococcal protein A promotes osteoclastogenesis through MAPK signaling during bone infection. *J Cell Physiol* 232:2396-2406.

23. Josse J, Valour F, Maali Y, Diot A, Batailler C, Ferry T, Laurent F. 2019. Interaction Between Staphylococcal Biofilm and Bone: How Does the Presence of Biofilm Promote Prosthesis Loosening? *Front Microbiol* 10:1602.
24. Wagner C, Hansch GM. 2017. Mechanisms of Bacterial Colonization of Implants and Host Response. *Adv Exp Med Biol* 971:15-27.
25. Burdette DL, Vance RE. 2013. STING and the innate immune response to nucleic acids in the cytosol. *Nat Immunol* 14:19-26.
26. Smith JA. 2020. STING, the Endoplasmic Reticulum, and Mitochondria: Is Three a Crowd or a Conversation? *Front Immunol* 11:611347.
27. Saxton RA, Sabatini DM. 2017. mTOR Signaling in Growth, Metabolism, and Disease. *Cell* 169:361-371.
28. Herzig S, Shaw RJ. 2018. AMPK: guardian of metabolism and mitochondrial homeostasis. *Nat Rev Mol Cell Biol* 19:121-135.
29. Lampropoulou V, Sergushichev A, Bambouskova M, Nair S, Vincent EE, Loginicheva E, Cervantes-Barragan L, Ma X, Huang SC, Griss T, Weinheimer CJ, Khader S, Randolph GJ, Pearce EJ, Jones RG, Diwan A, Diamond MS, Artyomov MN. 2016. Itaconate Links Inhibition of Succinate Dehydrogenase with Macrophage Metabolic Remodeling and Regulation of Inflammation. *Cell Metab* 24:158-166.
30. O'Neill LAJ, Artyomov MN. 2019. Itaconate: the poster child of metabolic reprogramming in macrophage function. *Nat Rev Immunol* 19:273-281.
31. Helming L, Gordon S. 2009. Molecular mediators of macrophage fusion. *Trends Cell Biol* 19:514-522.
32. Miyamoto H, Katsuyama E, Miyauchi Y, Hoshi H, Miyamoto K, Sato Y, Kobayashi T, Iwasaki R, Yoshida S, Mori T, Kanagawa H, Fujie A, Hao W, Morioka H, Matsumoto M, Toyama Y, Miyamoto T. 2012. An essential role for STAT6-STAT1 protein signaling in promoting macrophage cell-cell fusion. *J Biol Chem* 287:32479-32484.
33. Murray PJ. 2006. Understanding and exploiting the endogenous interleukin-10/STAT3-mediated anti-inflammatory response. *Curr Opin Pharmacol* 6:379-386.
34. Kumaran Satyanarayanan S, El Kebir D, Soboh S, Butenko S, Sekheri M, Saadi J, Peled N, Assi S, Othman A, Schif-Zuck S, Feuermann Y, Barkan D, Sher N, Filep JG, Ariel A. 2019. IFN-beta is a macrophage-derived effector cytokine facilitating the resolution of bacterial inflammation. *Nat Commun* 10:3471.
35. Feng X. 2005. RANKing intracellular signaling in osteoclasts. *IUBMB Life* 57:389-395.
36. Xiong Q, Zhang L, Ge W, Tang P. 2016. The roles of interferons in osteoclasts and osteoclastogenesis. *Joint Bone Spine* 83:276-281.
37. Christensen GD, Simpson WA, Younger JJ, Baddour LM, Barrett FF, Melton DM, Beachey EH. 1985. Adherence of coagulase-negative staphylococci to plastic tissue culture plates: a quantitative model for the adherence of staphylococci to medical devices. *J Clin Microbiol* 22:996-1006.
38. Beenken KE, Blevins JS, Smeltzer MS. 2003. Mutation of sarA in *Staphylococcus aureus* limits biofilm formation. *Infect Immun* 71:4206-4211.
39. Gillaspay AF, Hickmon SG, Skinner RA, Thomas JR, Nelson CL, Smeltzer MS. 1995. Role of the accessory gene regulator (agr) in pathogenesis of staphylococcal osteomyelitis. *Infect Immun* 63:3373-3380.



40. Thurlow LR, Hanke ML, Fritz T, Angle A, Aldrich A, Williams SH, Engebretsen IL, Bayles KW, Horswill AR, Kielian T. 2011. Staphylococcus aureus biofilms prevent macrophage phagocytosis and attenuate inflammation in vivo. *J Immunol* 186:6585-6596.
41. Bernthal NM, Pribaz JR, Stavrakis AI, Billi F, Cho JS, Ramos RI, Francis KP, Iwakura Y, Miller LS. 2011. Protective role of IL-1beta against post-arthroplasty Staphylococcus aureus infection. *J Orthop Res* 29:1621-1626.
42. Alboslemy T, Yu B, Rogers T, Kim MH. 2019. Staphylococcus aureus Biofilm-Conditioned Medium Impairs Macrophage-Mediated Antibiofilm Immune Response by Upregulating KLF2 Expression. *Infect Immun* 87:
43. Herbert S, Ziebandt AK, Ohlsen K, Schafer T, Hecker M, Albrecht D, Novick R, Gotz F. 2010. Repair of global regulators in Staphylococcus aureus 8325 and comparative analysis with other clinical isolates. *Infect Immun* 78:2877-2889.
44. Yang K, Xu J, Fan M, Tu F, Wang X, Ha T, Williams DL, Li C. 2020. Lactate Suppresses Macrophage Pro-Inflammatory Response to LPS Stimulation by Inhibition of YAP and NF-kappaB Activation via GPR81-Mediated Signaling. *Front Immunol* 11:587913.
45. Ratter JM, Rooijackers HMM, Hooiveld GJ, Hijmans AGM, de Galan BE, Tack CJ, Stienstra R. 2018. In vitro and in vivo Effects of Lactate on Metabolism and Cytokine Production of Human Primary PBMCs and Monocytes. *Front Immunol* 9:2564.
46. Errea A, Cayet D, Marchetti P, Tang C, Kluza J, Offermanns S, Sirard JC, Rumbo M. 2016. Lactate Inhibits the Pro-Inflammatory Response and Metabolic Reprogramming in Murine Macrophages in a GPR81-Independent Manner. *PLoS One* 11:e0163694.
47. Heim CE, Bosch ME, Yamada KJ, Aldrich AL, Chaudhari SS, Klinkebiel D, Gries CM, Alqarzaee AA, Li Y, Thomas VC, Seto E, Karpf AR, Kielian T. 2020. Lactate production by Staphylococcus aureus biofilm inhibits HDAC11 to reprogramme the host immune response during persistent infection. *Nat Microbiol* 5:1271-1284.
48. Scumpia PO, Botten GA, Norman JS, Kelly-Scumpia KM, Spreafico R, Ruccia AR, Purbey PK, Thomas BJ, Modlin RL, Smale ST. 2017. Opposing roles of Toll-like receptor and cytosolic DNA-STING signaling pathways for Staphylococcus aureus cutaneous host defense. *PLoS Pathog* 13:e1006496.
49. Sun L, Wu J, Du F, Chen X, Chen ZJ. 2013. Cyclic GMP-AMP synthase is a cytosolic DNA sensor that activates the type I interferon pathway. *Science* 339:786-791.
50. Takaoka A, Wang Z, Choi MK, Yanai H, Negishi H, Ban T, Lu Y, Miyagishi M, Kodama T, Honda K, Ohba Y, Taniguchi T. 2007. DAI (DLM-1/ZBP1) is a cytosolic DNA sensor and an activator of innate immune response. *Nature* 448:501-505.
51. Hopfner KP, Hornung V. 2020. Molecular mechanisms and cellular functions of cGAS-STING signalling. *Nat Rev Mol Cell Biol* 21:501-521.
52. Gries CM, Bruger EL, Moormeier DE, Scherr TD, Waters CM, Kielian T. 2016. Cyclic di-AMP Released from Staphylococcus aureus Biofilm Induces a Macrophage Type I Interferon Response. *Infect Immun* 84:3564-3574.
53. Burdette DL, Monroe KM, Sotelo-Troha K, Iwig JS, Eckert B, Hyodo M, Hayakawa Y, Vance RE. 2011. STING is a direct innate immune sensor of cyclic di-GMP. *Nature* 478:515-518.
54. Martin FJ, Gomez MI, Wetzel DM, Memmi G, O'Seaghda M, Soong G, Schindler C, Prince A. 2009. Staphylococcus aureus activates type I IFN signaling in mice and humans through the Xr repeated sequences of protein A. *J Clin Invest* 119:1931-1939.

55. Yang J, Ryu YH, Yun CH, Han SH. 2009. Impaired osteoclastogenesis by staphylococcal lipoteichoic acid through Toll-like receptor 2 with partial involvement of MyD88. *J Leukoc Biol* 86:823-831.
56. Putnam NE, Fulbright LE, Curry JM, Ford CA, Petronglo JR, Hendrix AS, Cassat JE. 2019. MyD88 and IL-1R signaling drive antibacterial immunity and osteoclast-driven bone loss during *Staphylococcus aureus* osteomyelitis. *PLoS Pathog* 15:e1007744.
57. Kim J, Yang J, Park OJ, Kang SS, Kim WS, Kurokawa K, Yun CH, Kim HH, Lee BL, Han SH. 2013. Lipoproteins are an important bacterial component responsible for bone destruction through the induction of osteoclast differentiation and activation. *J Bone Miner Res* 28:2381-2391.
58. AlQranei MS, Senbanjo LT, Aljohani H, Hamza T, Chellaiah MA. 2021. Lipopolysaccharide-TLR-4 Axis regulates Osteoclastogenesis independent of RANKL/RANK signaling. *BMC Immunol* 22:23.
59. Zou W, Schwartz H, Endres S, Hartmann G, Bar-Shavit Z. 2002. CpG oligonucleotides: novel regulators of osteoclast differentiation. *FASEB J* 16:274-282.
60. Zou W, Bar-Shavit Z. 2002. Dual modulation of osteoclast differentiation by lipopolysaccharide. *J Bone Miner Res* 17:1211-1218.
61. Takami M, Kim N, Rho J, Choi Y. 2002. Stimulation by toll-like receptors inhibits osteoclast differentiation. *J Immunol* 169:1516-1523.
62. Liu J, Wang S, Zhang P, Said-Al-Naief N, Michalek SM, Feng X. 2009. Molecular mechanism of the bifunctional role of lipopolysaccharide in osteoclastogenesis. *J Biol Chem* 284:12512-12523.
63. Souza PPC, Lerner UH. 2019. Finding a Toll on the Route: The Fate of Osteoclast Progenitors After Toll-Like Receptor Activation. *Front Immunol* 10:1663.
64. Hayashi T, Kaneda T, Toyama Y, Kumegawa M, Hakeda Y. 2002. Regulation of receptor activator of NF-kappa B ligand-induced osteoclastogenesis by endogenous interferon-beta (INF-beta ) and suppressors of cytokine signaling (SOCS). The possible counteracting role of SOCSs- in IFN-beta-inhibited osteoclast formation. *J Biol Chem* 277:27880-27886.
65. Taubmann J, Krishnacoumar B, Bohm C, Faas M, Muller DIH, Adam S, Stoll C, Bottcher M, Mougiakakos D, Sonnewald U, Hofmann J, Schett G, Kronke G, Scholtyssek C. 2020. Metabolic reprogramming of osteoclasts represents a therapeutic target during the treatment of osteoporosis. *Sci Rep* 10:21020.
66. Pereira M, Petretto E, Gordon S, Bassett JHD, Williams GR, Behmoaras J. 2018. Common signalling pathways in macrophage and osteoclast multinucleation. *J Cell Sci* 131:
67. Miron RJ, Bosshardt DD. 2018. Multinucleated Giant Cells: Good Guys or Bad Guys? *Tissue Eng Part B Rev* 24:53-65.
68. Moreno JL, Mikhailenko I, Tondravi MM, Keegan AD. 2007. IL-4 promotes the formation of multinucleated giant cells from macrophage precursors by a STAT6-dependent, homotypic mechanism: contribution of E-cadherin. *J Leukoc Biol* 82:1542-1553.
69. Le KY, Villaruz AE, Zheng Y, He L, Fisher EL, Nguyen TH, Ho TV, Yeh AJ, Joo HS, Cheung GYC, Otto M. 2019. Role of Phenol-Soluble Modulins in *Staphylococcus epidermidis* Biofilm Formation and Infection of Indwelling Medical Devices. *J Mol Biol* 431:3015-3027.

70. Kretschmer D, Gleske AK, Rautenberg M, Wang R, Koberle M, Bohn E, Schoneberg T, Rabiet MJ, Boulay F, Klebanoff SJ, van Kessel KA, van Strijp JA, Otto M, Peschel A. 2010. Human formyl peptide receptor 2 senses highly pathogenic *Staphylococcus aureus*. *Cell Host Microbe* 7:463-473.
71. Schlatterer K, Beck C, Hanzelmann D, Lebtig M, Fehrenbacher B, Schaller M, Ebner P, Nega M, Otto M, Kretschmer D, Peschel A. 2018. The Mechanism behind Bacterial Lipoprotein Release: Phenol-Soluble Modulins Mediate Toll-Like Receptor 2 Activation via Extracellular Vesicle Release from *Staphylococcus aureus*. *mBio* 9:
72. Kelly B, O'Neill LA. 2015. Metabolic reprogramming in macrophages and dendritic cells in innate immunity. *Cell Res* 25:771-784.
73. Yamada KJ, Heim CE, Xi X, Attri KS, Wang D, Zhang W, Singh PK, Bronich TK, Kielian T. 2020. Monocyte metabolic reprogramming promotes pro-inflammatory activity and *Staphylococcus aureus* biofilm clearance. *PLoS Pathog* 16:e1008354.
74. Li B, Lee WC, Song C, Ye L, Abel ED, Long F. 2020. Both aerobic glycolysis and mitochondrial respiration are required for osteoclast differentiation. *FASEB J* 34:11058-11067.
75. Indo Y, Takeshita S, Ishii KA, Hoshii T, Aburatani H, Hirao A, Ikeda K. 2013. Metabolic regulation of osteoclast differentiation and function. *J Bone Miner Res* 28:2392-2399.
76. Ip WKE, Hoshi N, Shouval DS, Snapper S, Medzhitov R. 2017. Anti-inflammatory effect of IL-10 mediated by metabolic reprogramming of macrophages. *Science* 356:513-519.
77. Van den Bossche J, Baardman J, Otto NA, van der Velden S, Neele AE, van den Berg SM, Luque-Martin R, Chen HJ, Boshuizen MC, Ahmed M, Hoeksema MA, de Vos AF, de Winther MP. 2016. Mitochondrial Dysfunction Prevents Repolarization of Inflammatory Macrophages. *Cell Rep* 17:684-696.
78. Aki T, Funakoshi T, Noritake K, Unuma K, Uemura K. 2020. Extracellular glucose is crucially involved in the fate decision of LPS-stimulated RAW264.7 murine macrophage cells. *Sci Rep* 10:10581.
79. Raschke WC, Baird S, Ralph P, Nakoinz I. 1978. Functional macrophage cell lines transformed by Abelson leukemia virus. *Cell* 15:261-267.

## Figure Legends

**Fig. 1 Early immune response of macrophages towards conditioned media.** RAW264.7 cells were cultivated in CM 1:1 diluted in fresh growth media (DMEM high glucose + 10% FCS + 1% Pen/Strep) and immune function was investigated. A) Surface marker profile of macrophages. Cells were stimulated with CM for 20 hours and surface protein levels of relevant TLRs, MHC complex II and co-stimulatory proteins were measured by FACS analysis. Data are presented as median expression levels measured by fluorescence intensity. n=5 experiments, p-values are calculated by Mann-Whitney U test. B) Gene expression analysis of relevant cytokines. Cells were stimulated with CM for 4 hours and mRNA levels of pro- (IL-1 $\beta$ , IL-6, TNF- $\alpha$  and IFN- $\beta$ ) and anti-inflammatory (IL-10) cytokines were quantified by RT-qPCR. Data are presented as relative gene expression of gene of interest related to the reference gene HPRT-1. n=5 experiments, p-values are calculated by Mann-Whitney U test. C) Protein amounts of relevant cytokines in the supernatant. Cells were stimulated with CM for 20 hours and protein concentration of pro- (IL-1 $\alpha$ , IL-6, TNF- $\alpha$  and IFN- $\beta$ ) and anti-inflammatory (IL-10) cytokines were quantified in the supernatant by multi cytokine bead array (CBA; LegendPlex). Data are presented as absolute concentration (pg/ml). n=5 experiments, p-values are calculated by Mann-Whitney U test. D) Activation of NF- $\kappa$ B and IRF-3 signaling in macrophages. Cells were stimulated with CM for 4 hours and presence of phospho-NF $\kappa$ B p65 and phospho-IRF3 as activated forms of the transcription factors was visualized by Western Blot. HSP90 was used as loading control. PC: positive control (1  $\mu$ g Pam3CSK4 + 100 nM CpG), n=4 experiments. E) Free bacterial DNA content in CM. DNA was extracted from 1 ml CM and amplified by qPCR using SA specific primers for gyrase B (product length: 147 bp) and SE specific primers for gyrase A (product length: 194 bp). PCR products were visualized by agarose gel electrophoresis. Numbers below bands show the mean Ct value of n=3 CM approaches. F) Cell stress/ ROS production of macrophages. Cells were stimulated with CM for 2 hours and cell stress was measured by FACS analysis using an oxidative stress reagent. Data are presented as median ROS production measured by fluorescence intensity. n=4 experiments. G) Phagocytic activity of macrophages. Cells were stimulated with CM for 24 hours and phagocytic uptake of fluorescence coupled beads was investigated by FACS analysis. Data are presented as median bead uptake measured by fluorescence intensity. n=5 experiments (one experiment was excluded from statistics as overall intensities were much higher but showed the same trend). A-C+F+G) A positive control (PC) was included in each respective experiment and data are shown in Suppl. Fig. 4.

**Fig. 2 Early metabolic changes in macrophages by conditioned media.** RAW264.7 cells were cultivated in CM 1:1 diluted in fresh growth media (DMEM high glucose + 10% FCS + 1%

Pen/Strep) and metabolic parameters for glycolysis and OxPhos were investigated. A) L-lactate amount in conditioned media. Bacteria were cultivated either in planktonic culture for 24 hours or biofilm culture for 6 days. CM were harvested and L-lactate concentration was quantified by an enzyme-based assay. Data are presented as concentration (mM) measured by bioluminescent light release. n=5 experiments. B) L-lactate secretion by macrophages. Cells were stimulated with CM 1:1 diluted in fresh growth media for 24 hours. Total L-lactate in the supernatant was quantified by an enzyme-based assay. Amount of L-lactate released by macrophages was calculated by total L-lactate of macrophage supernatants minus L-lactate of CM 1:1 diluted in fresh growth media. Data are presented as concentration (mM) measured by bioluminescent light release. n=5 experiments, p-values are calculated by Mann-Whitney U test. C) Gene expression analysis of LDHA or MCT-1. Cells were stimulated with CM for 4 hours and mRNA levels of LDHA or MCT-1 were quantified by RT-qPCR. Data are presented as relative gene expression of gene of interest related to the reference gene HPRT-1. n=5 experiments. D) Protein levels of phospho-LDHA (upper blot) and MCT-1 (lower blot). Cells were stimulated with CM for 24 hours and presence of phospho-LDHA indicating stabilized protein or lactate transporter MCT-1 was visualized by Western Blot. HSP90 was used as loading control. PC: positive control (1  $\mu$ g Pam3CSK4 + 100 nM CpG), n=4 experiments. E) Activation of glycolysis and TCA pathway in macrophages. Cells were stimulated with CM for 24 hours and presence of phospho-4E-BP1 as down-stream target of mTORC1 pathway and marker for glycolysis and phospho-AMPK as activator of TCA cycle was visualized by Western Blot. B-Actin was used as loading control. PC: positive control (1  $\mu$ g Pam3CSK4 + 100 nM CpG), n=4 experiments. F) Gene expression analysis of ACOD-1. Cells were stimulated with CM for 4 hours and mRNA levels of ACOD-1 were quantified by RT-qPCR. Data are presented as relative gene expression of gene of interest related to the reference gene HPRT-1. n=5 experiments. G) Cell stress/ ROS production of macrophages. Cells were stimulated with CM for 24 hours and cell stress was measured by FACS analysis using an oxidative stress reagent. Data are presented as median ROS production measured by fluorescence intensity. n=4 experiments. H) Mitochondrial activity of macrophages. Cells were stimulated with CM for 24 hours and mitochondrial activity was measured by FACS analysis using a membrane potential-dependent fluorescent dye. Data are presented as median mitochondrial potential measured by fluorescence intensity. n=4 experiments, p-values are calculated by Mann-Whitney U test. I) ATP production by macrophages. Cells were stimulated with CM for 24 hours and total ATP content was measured in cell lysates by enzyme-based assay (CTG). Data are presented as relative light units measured by bioluminescent light release. n=4 experiments in triplicates (mean of triplicates was included in statistics). B+C+F-I) A positive control (PC) was included in each respective experiment and data are shown in Suppl. Fig. 4.

**Fig. 3 Effect of CM on RANKL-mediated osteoclastogenesis of macrophages.** RAW264.7 cells were cultivated in CM 1:1 diluted in fresh growth media (DMEM high glucose + 10% FCS + 1% Pen/Strep) and RANKL-induced osteoclastogenic differentiation was investigated. In experiments with a cultivation time above 2 days 50  $\mu$ M  $\beta$ -mercapto ethanol was added to the media to reduce cell proliferation and avoid overgrowing of the cells (here: OC formation after 5 days). A) Osteoclast formation. Cells were stimulated with CM and RANKL (50 ng/ml) for 5 days. At day 5 cells were fixed, stained for TRAP and nuclei and total numbers of formed osteoclasts (OC) per well were counted. Osteoclasts were defined as TRAP-positive multinucleated giant cells with at least 3 nuclei. Data are presented as OC numbers per well. n=5 experiments in duplicates (mean of duplicates was included in statistics), p-values are calculated by Mann-Whitney U test. B) Gene expression analysis of NFATc1. Cells were stimulated with CM and RANKL (50 ng/ml) for 2 days and mRNA levels of NFATc1 were quantified by RT-qPCR. Data are presented as relative gene expression of gene of interest related to the reference gene HPRT-1. n=5 experiments, p-values are calculated by Mann-Whitney U test. C) Protein levels of NFATc1. Cells were stimulated with CM and RANKL (50 ng/ml) for 2 days and presence of NFATc1 as master regulator of osteoclastogenesis was visualized by Western Blot. B-Actin was used as loading control. n=4 experiments. D) Visualization of formed osteoclasts after 5 days of differentiation. TRAP activity is shown by violet color development and nuclei are stained in blue. Upper picture is showing RANKL-induced osteoclast formation (positive control), lower picture is showing formed osteoclast additionally stimulated with SE planktonic CM. E-F) Gene expression analysis of TRAP (E) and fusion marker ATP6Vod2 (F). Cells were stimulated with CM and RANKL (50 ng/ml) for 2 days and mRNA levels of TRAP or ATP6Vod2 were quantified by RT-qPCR. Data are presented as relative gene expression of gene of interest related to the reference gene HPRT-1. n=5 experiments, p-values are calculated by Mann-Whitney U test.

**Fig. 4 MGC formation by macrophages stimulated with CM + RANKL and late immune response.** RAW264.7 cells were cultivated in CM 1:1 diluted in fresh growth media (DMEM high glucose + 10% FCS + 1% Pen/Strep) and CM + RANKL-induced multinucleated giant cell (MGC) formation was investigated. In experiments with a cultivation time above 2 days 50  $\mu$ M  $\beta$ -mercapto ethanol was added to the media to reduce cell proliferation and avoid overgrowing of the cells (here: MGC formation after 5 days). A) Cells were stimulated with CM and RANKL (50 ng/ml) for 5 days. At day 5 cells were fixed, stained for TRAP and nuclei and total numbers of formed MGCs per well were counted. MGCs were defined as TRAP-negative multinucleated giant cells with at least 3 nuclei. Data are presented as MGC numbers per well. n=5 experiments in duplicates (mean of duplicates was included in statistics), p-values are calculated by Mann-Whitney U test. B) Visualization of formed MGCs after 5 days of differentiation. TRAP activity is shown by violet color development and nuclei are stained in blue. Upper picture is showing spontaneous MGC formation in medium (negative control), lower picture is showing formed

MGCs stimulated with SE planktonic CM + RANKL. C) Activation of Stat6 and Stat3 signaling in macrophages. Cells were stimulated with CM and RANKL (50 ng/ml) for 2 days and presence of phospho-Stat6 and phospho-Stat3 as activated forms of the transcription factors was visualized by Western Blot. IL-4 and IL-10 (both: 25 ng/ml for 1 hour) were used as positive controls for respective Stat-pathway activation. B-Actin was used as loading control. n=4 experiments. D) Gene expression analysis of relevant cytokines. Cells were stimulated with CM and RANKL (50 ng/ml) for 2 days and mRNA levels of pro- (IL-1 $\beta$ , IL-6 and TNF- $\alpha$ ) and anti-inflammatory (IL-10 and IL-4) cytokines were quantified by RT-qPCR. Data are presented as relative gene expression of gene of interest related to the reference gene HPRT-1. n=5 experiments, p-values are calculated by Mann-Whitney U test. E) Protein amounts of relevant cytokines in the supernatant. Cells were stimulated with CM and RANKL (50 ng/ml) for 2 days and protein concentration of pro- (IL-1 $\alpha$ , IL-6, TNF- $\alpha$  and IFN- $\beta$ ) and anti-inflammatory (IL-10) cytokines were quantified in the supernatant by multi cytokine bead array (CBA; LegendPlex). Data are presented as absolute concentration (pg/ml). n=5 experiments, p-values are calculated by Mann-Whitney U test. F) Gene expression analysis of iNOS. Cells were stimulated with CM and RANKL (50 ng/ml) for 2 days and mRNA levels of iNOS were quantified by RT-qPCR. Data are presented as relative gene expression of gene of interest related to the reference gene HPRT-1. n=5 experiments, p-values are calculated by Mann-Whitney U test. G) NO release by macrophages. Cells were stimulated with CM and RANKL (50 ng/ml) for 2 days and NO content in the supernatant was quantified by Griess reaction. Data are presented as concentration ( $\mu$ M) calculated by OD at 540 nm. n=5 experiments, p-values are calculated by Mann-Whitney U test.

**Fig. 5 Metabolic changes during macrophage differentiation stimulated with CM + RANKL.**

RAW264.7 cells were cultivated in CM 1:1 diluted in fresh growth media (DMEM high glucose + 10% FCS + 1% Pen/Strep) and effect of CM + RANKL stimulation on macrophage immune metabolism was investigated. In experiments with a cultivation time above 2 days 50  $\mu$ M  $\beta$ -mercapto ethanol was added to the media to reduce cell proliferation and avoid overgrowing of the cells (here: Mito copy No. and mitochondrial activity after 4 days). A) Number of mitochondria per macrophage. Cells were stimulated with CM and RANKL (50 ng/ml) for 4 days and mitochondria copy numbers were quantified by quantitative PCR. Data are presented as mitochondrial DNA (mtDNA) copies related to nuclear DNA (nDNA). n=4 experiments, p-values are calculated by Mann-Whitney U test. B) Mitochondrial activity of macrophages. Cells were stimulated with CM and RANKL (50 ng/ml) for 4 days and mitochondrial activity was measured by FACS analysis using a membrane potential-dependent fluorescent dye. Data are presented as median mitochondrial potential measured by fluorescence intensity. n=4 experiments, p-values are calculated by Mann-Whitney U test. C) Activation of glycolysis and TCA pathway in macrophages. Cells were stimulated with CM and RANKL (50 ng/ml) for 2 days and presence of phospho-4E-BP1 as down-stream target of mTORC1 pathway and marker for glycolysis and

phospho-AMPK as activator of TCA cycle was visualized by Western Blot. B-Actin was used as loading control. n=4 experiments. D) Protein levels of OxPhos complexes. Cells were stimulated with CM and RANKL (50 ng/ml) for 2 days and presence of OxPhos complexes I-V was visualized by Western Blot. HSP-90 was used as loading control. n=4 experiments.

**Fig. 6 Effect of stimulation with TLR-ligands or cytokines on differentiation and late immune response of macrophages.** RAW264.7 cells were cultivated in growth media (DMEM high glucose + 10% FCS + 1% Pen/Strep) and effect of TLR-ligands (TLR-2: Pam3CSK4, P3 1 µg/ml, TLR-9: CpG 100 nM) or cytokines (IL-10 or TNF-α, both 25 ng/ml) ± RANKL stimulation on macrophage differentiation and late immune response was investigated. In experiments with a cultivation time above 2 days 50 µM β-mercapto ethanol was added to the media to reduce cell proliferation and avoid overgrowing of the cells (here: OC/MGC formation after 5 days). A+B) Cells were stimulated with different stimuli ± RANKL (50 ng/ml) for 5 days. At day 5 cells were fixed, stained for TRAP and nuclei and total numbers of formed osteoclasts (A) or MGCs (B) per well were counted. Osteoclasts were defined as TRAP-positive multinucleated giant cells with at least 3 nuclei. MGCs were defined as TRAP-negative multinucleated giant cells with at least 3 nuclei. Data are presented as OC / MGC numbers per well. n=3 experiments in duplicates, mean + SD are shown. C) Morphological appearance of formed OC and MGC in TRAP/nuclei stain after stimulation with CpG + RL for 5 days. D-F) Gene expression analysis of NFATc1 as osteoclastogenesis marker (D) and pro- (TNF-α, E) and anti- (IL-10, F) inflammatory cytokines. Cells were stimulated with different stimuli and RANKL (50 ng/ml) for 2 days and mRNA levels of NFATc1, TNF-α and IL-10 were quantified by RT-qPCR. Data are presented as relative gene expression of gene of interest related to the reference gene HPRT-1. n=3 experiments, mean + SD are shown. G) Activation of Stat3 signaling in macrophages. Cells were stimulated with different stimuli and RANKL (RL; 50 ng/ml) for 2 days and presence of phospho-Stat3 as activated form of the transcription factor was visualized by Western Blot. IL-10 stimulation (25 ng/ml for 1 hour) was used as positive control for Stat3-pathway activation. B-Actin was used as loading control. n=3 experiments.

**Fig. 7 Effect of IFN-β on osteoclastogenic differentiation of macrophages.** RAW264.7 cells were cultivated in growth media (DMEM high glucose + 10% FCS + 1% Pen/Strep) and effect of IFN-β in different concentrations (20, 200 pg/ml and 2 ng/ml) ± RANKL stimulation on macrophage osteoclastogenesis was analyzed. In experiments with a cultivation time above 2 days, 50 µM β-mercapto ethanol was added to the media to reduce cell proliferation and avoid overgrowing of the cells. Additionally, a half media exchange and restimulation were performed late day 2 or early day 3 (here: OC formation after 5 days). A) Cells were cultivated with different



concentrations of IFN- $\beta$   $\pm$  RANKL (50 ng/ml) for 5 days. At day 5 cells were fixed, stained for TRAP and nuclei and total numbers of formed osteoclasts per well were counted. Osteoclasts were defined as TRAP-positive multinucleated giant cells with at least 3 nuclei. Data are presented as OC numbers per well. n=4 experiments in duplicates (mean of duplicates was included in statistics), p-value is calculated by Kruskal-Wallis test. B+C) Expression analysis of osteoclastogenic marker genes for NFATc1, TRAP and ATP6Vod2 (B) and IFN- $\beta$  target gene ISG15 (C). Cells were stimulated with different IFN- $\beta$  concentrations and RANKL (50 ng/ml) for 2 days and mRNA levels of NFATc1, TRAP, ATP6Vod2 or ISG15 were quantified by RT-qPCR. Data are presented as relative gene expression of gene of interest related to the reference gene HPRT-1. n=4 experiments, p-values are calculated by Kruskal-Wallis test. D) Cell density after 5 days cultivation. Cells were cultivated with and without 2 ng/ml IFN- $\beta$  for 5 days (controls of TRAP assay). At day 5 cells were fixed and stained for nuclei. Cells are presented as dark spots after hematoxylin stain. Representative pictures of n=4 experiments in duplicates are shown. E) Activation of Stat1 signaling in macrophages by IFN- $\beta$  at different concentrations. In order to test activity of IFN- $\beta$ , cells were stimulated with different IFN- $\beta$  concentration (100 pg/ml and 1, 10, 100 ng/ml) for 1 hour and presence of phospho-Stat1 as activated form of the transcription factor was visualized by Western Blot. B-Actin was used as loading control. n=1 experiment.

**Fig. 8 Effect of extracellular lactate on osteoclastogenic differentiation of macrophages.**

RAW264.7 cells were cultivated in growth media (DMEM high glucose + 10% FCS + 1% Pen/Strep) and effect of added L- or D-lactate in different concentrations (5, 10, 15 or 20 mM)  $\pm$  RANKL stimulation on macrophage osteoclastogenesis and metabolism was investigated. In experiments with a cultivation time above 2 days, 50  $\mu$ M  $\beta$ -mercapto ethanol was added to the media to reduce cell proliferation and avoid overgrowing of the cells. Additionally, a half media exchange and restimulation were performed late day 2 and early day 5 (here: OC/MGC formation after 6 days). A+B) Cells were cultivated with different concentrations of L-lactate  $\pm$  RANKL (50 ng/ml) for 6 days. At day 6 cells were fixed, stained for TRAP and nuclei and total numbers of formed osteoclasts per well were counted. A) shows morphological appearance of formed OC. B) shows osteoclast numbers per well. Osteoclasts were defined as TRAP-positive multinucleated giant cells with at least 3 nuclei. Data are presented as OC numbers per well. n=3 experiments in duplicates, mean + SD are shown. C) Gene expression analysis of osteoclastogenesis markers NFATc1, TRAP and ATP6Vod2. Cells were stimulated with different L-lactate concentrations and RANKL (50 ng/ml) for 2 days and mRNA levels of NFATc1, TRAP or ATP6Vod2 were quantified by RT-qPCR. Data are presented as relative gene expression of gene of interest related to the reference gene HPRT-1. n=4 experiments, mean + SD are shown. D) Activation of glycolysis and TCA pathway in macrophages. Cells were stimulated with different L-lactate concentrations and RANKL (50 ng/ml) for 2 days and presence of phospho-4E-BP1 as down-stream target of mTORC1 pathway and marker for glycolysis and phospho-AMPK as

activator of TCA cycle was visualized by Western Blot. HSP90 was used as loading control. n=3 experiments. E) Gene expression analysis of osteoclastogenesis markers NFATc1, TRAP and ATP6Vod2. Cells were stimulated with different D-lactate concentrations (10 and 20 mM) and RANKL (50 ng/ml) for 2 days and mRNA levels of NFATc1, TRAP or ATP6Vod2 were quantified by RT-qPCR. Data are presented as relative gene expression of gene of interest related to the reference gene HPRT-1. n=3 experiments, mean + SD are shown. F+G) Gene expression analysis of LDHA (F) or MCT-1 (G). Cells were stimulated with different L- (left graph) or D-lactate (right graph) concentrations and RANKL (50 ng/ml) for 2 days and mRNA levels of LDHA or MCT-1 were quantified by RT-qPCR. Data are presented as relative gene expression of gene of interest related to the reference gene HPRT-1. n=3 experiments, mean + SD are shown.

**Table 1** List of oligonucleotides used for quantitative RT-PCR analysis.

<b>Gene for</b>	<b>RefSeq</b>	<b>Forward primer</b>	<b>Reverse primer</b>
ACOD-1	NM_008392.1	CAGCTCTATCGGAAGCCCTG	CAGAAACTTGGACGCAGCAG
HPRT-1	NM_013556.2	GGGGACATAAAAAGTTATTGGTGG	CATTTTGGGGCTGTACTGCT
IFN- $\beta$	NM_010510.1	TGGGAGATGTCCTCAACTGC	CCAGGCGTAGCTGTTGTACT
IL-10	NM_010548.2	GGTTGCCAAGCCTTATCGGA	ACCTGCTCCACTGCCTTGCT
IL-1 $\beta$	NM_008361.4	ACTCATTGTGGCTGTGGAGAAG	GCCGTCTTTCATTACACAGGAC
IL-4	NM_021283.2	GAGCTGCAGAGACTCTTTCG	TCAGTGATGTGGACTTGGACT
IL-6	NM_031168.2	CCGGAGAGGAGACTTCACAG	TTCTGCAAGTGCATCATCGT
iNOS ( <i>Nos2</i> )	NM_010927.4	CATGAGCTTGGTGTGGGTG	TCCGCAAATGTAGAGGTGGC
LDHA	NM_010699.2	CAGGCTCCCCAGAACAAGAT	CAACAAGGGCAAGCTCATCC
MCT-1 ( <i>Slc16A1</i> )	NM_009196.4	GTGACCATTGTGGAATGCTG	CTCCGCTTCTGTTCTTTGG
NFATc1	NM_016791.4	CAGGGCTCACTATGAGACGG	AGCTGTAGCGTGAGAGGT
TNF- $\alpha$	NM_013693.3	AAAATTCGAGTGACAAGCCTGTAG	CCCTGAAGAGAACCTGGGAGTAG
TRAP ( <i>Acp5</i> )	NM_001102405.1	TTCCAGGAGACCTTTGAGGA	GGTAGTAAGGGCTGGGGAAG

Mouse specific primers were designed intron-flanking and included all transcript variants if possible and were obtained from biomers.net GmbH, Germany. If more transcript variants are present, RefSeq is given for transcript variant 1. Gene name is shown in brackets if different from protein name.

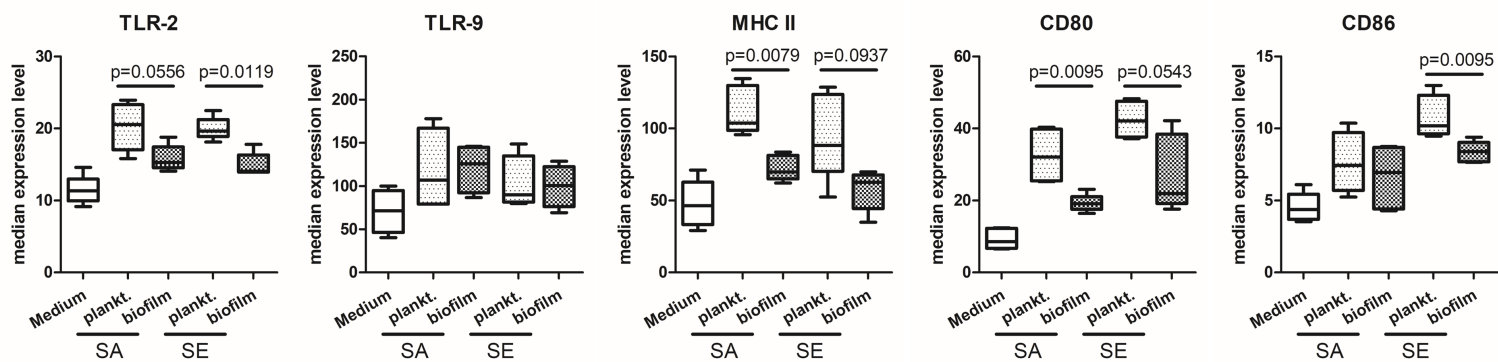
**Table 2 List of antibodies used for Immunoblotting (Western Blot).**

<b>Protein</b>	<b>Source</b>	<b>Size (kDa)</b>	<b>Dilution</b>	<b>Company</b>
$\beta$ -Actin	rabbit	42	1:1000	Proteintech, USA
HSP-90	rabbit	90	1:1000	Cell Signaling Technology, USA
MCT-1	rabbit	38-45	1:3000	Proteintech, USA
NFAT1	rabbit	140	1:500	Cell Signaling Technology, USA
Phospho-AMPK $\alpha$ (Thr172)	rabbit	62	1:1000	Cell Signaling Technology, USA
Phospho-4E-BP1 (Thr37/46)	rabbit	15-20	1:1000	Cell Signaling Technology, USA
Phospho-IRF3 (Ser396)	rabbit	45-55	1:1000	Cell Signaling Technology, USA
Phospho-LDHA (Tyr10)	rabbit	37	1:1000	Cell Signaling Technology, USA
Phospho-NF $\kappa$ B p65 (Ser536)	rabbit	65	1:1000	Cell Signaling Technology, USA
Phospho-Stat3 (Tyr705)	rabbit	79, 86	1:1000	Cell Signaling Technology, USA
Phospho-Stat6 (Tyr641)	rabbit	110	1:1000	Cell Signaling Technology, USA
Total OXPHOS (CI-V)	mouse	20, 30, 40, 48, 55	1:1000	Abcam, UK
Anti-mouse IgG, HRP-linked	horse		1:1000	Cell Signaling Technology, USA
Anti-rabbit IgG, HRP-linked	goat		1:1000	Cell Signaling Technology, USA

Antibodies were all recommended for use in mouse and applied according to the manufacturer's advice. Proteins were detected by chemiluminescent luminol reaction after incubation with respective HRP-linked secondary antibody and imaged in a ChemoStar ECL Imager.

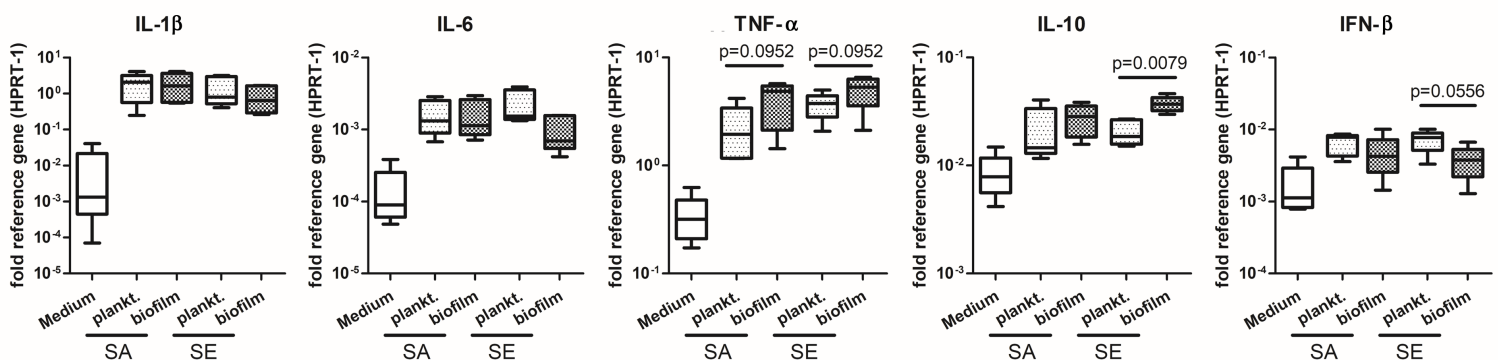
**A**

**FACS**



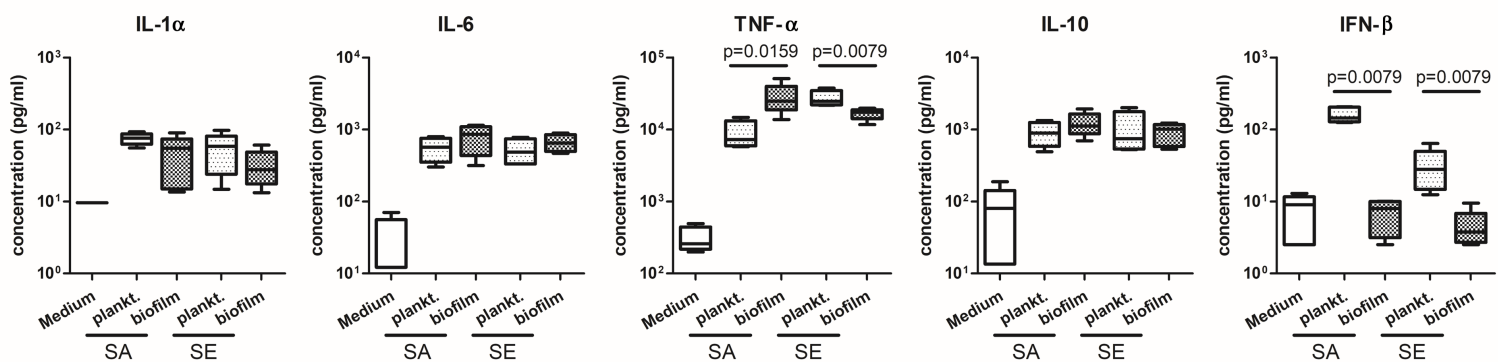
**B**

**qPCR**

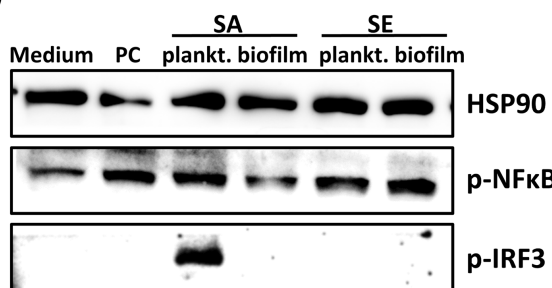


**C**

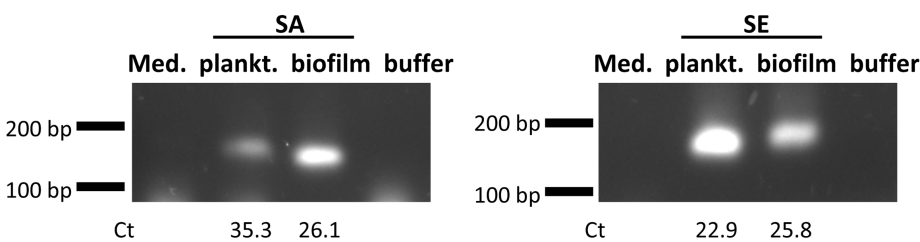
**CBA**



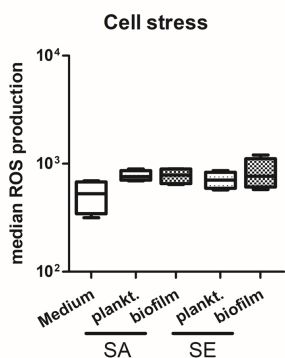
**D**



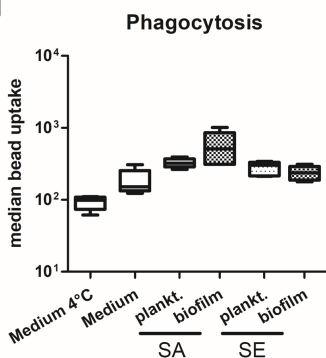
**E**

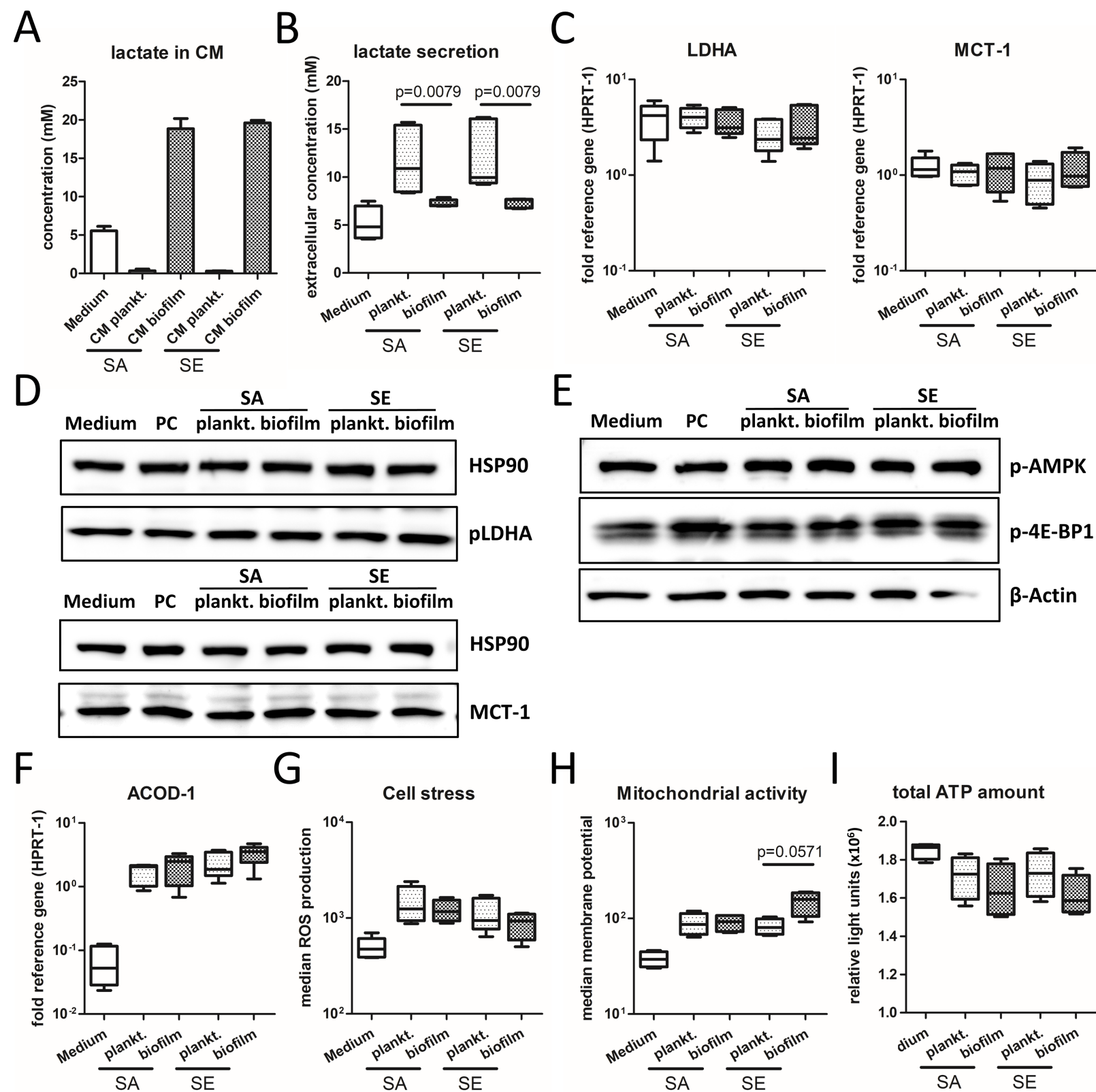


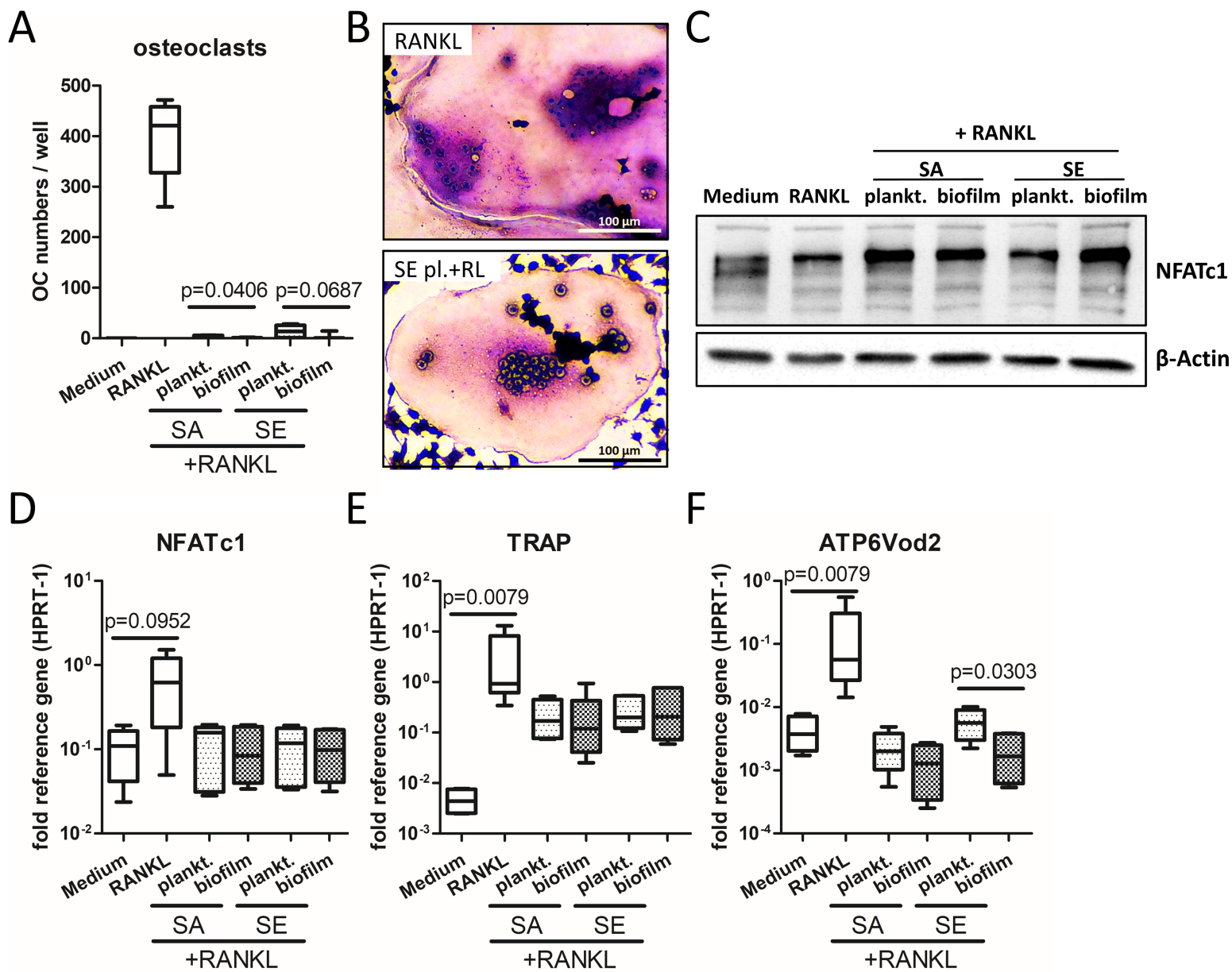
**F**



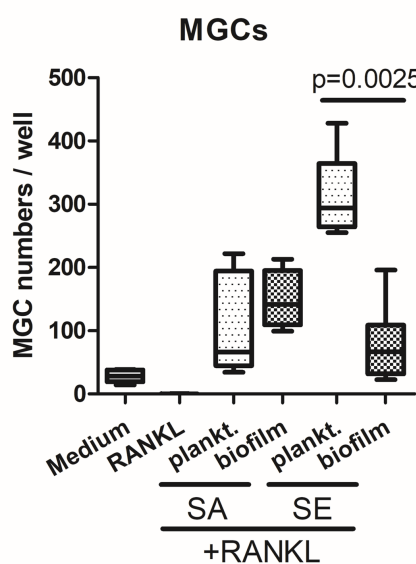
**G**



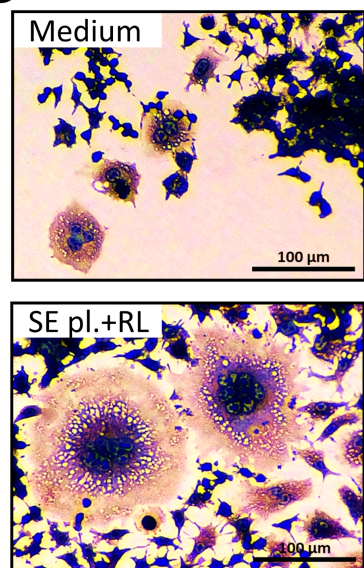




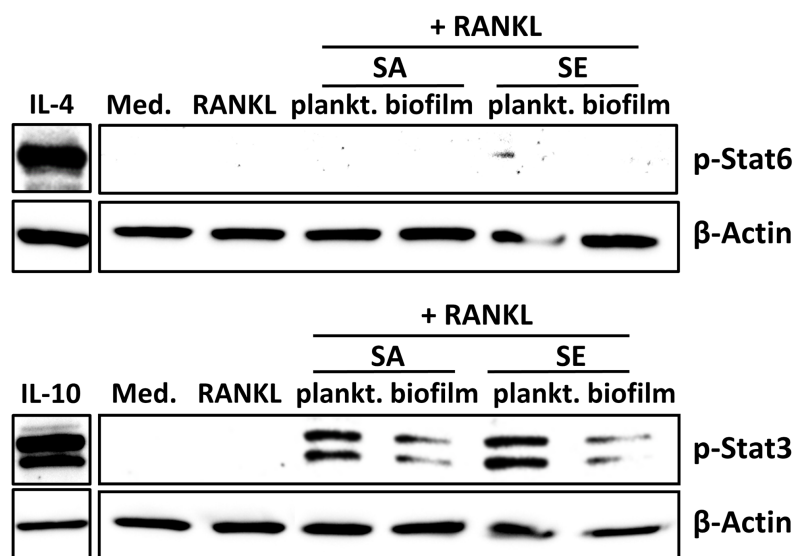
**A**



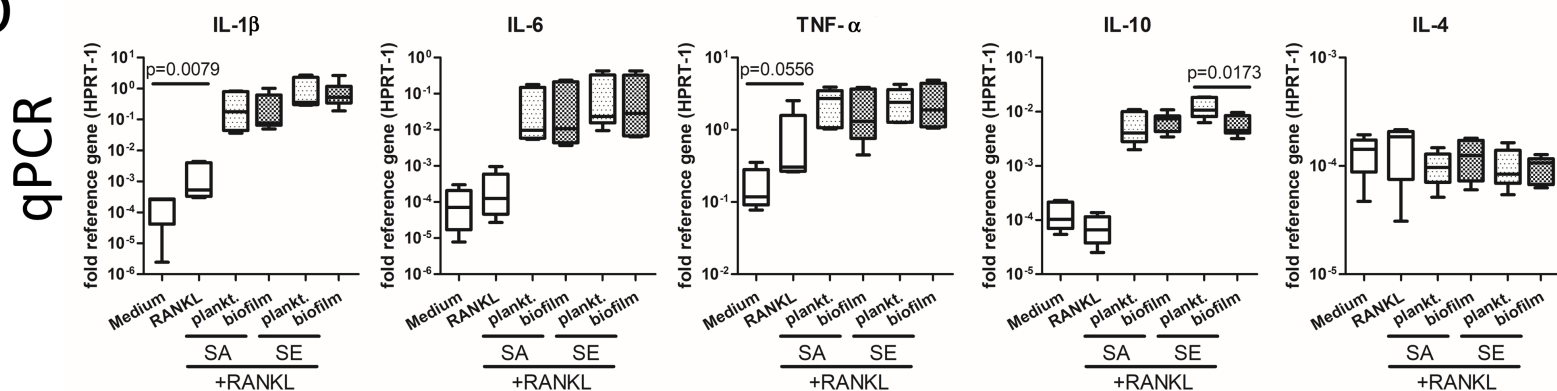
**B**



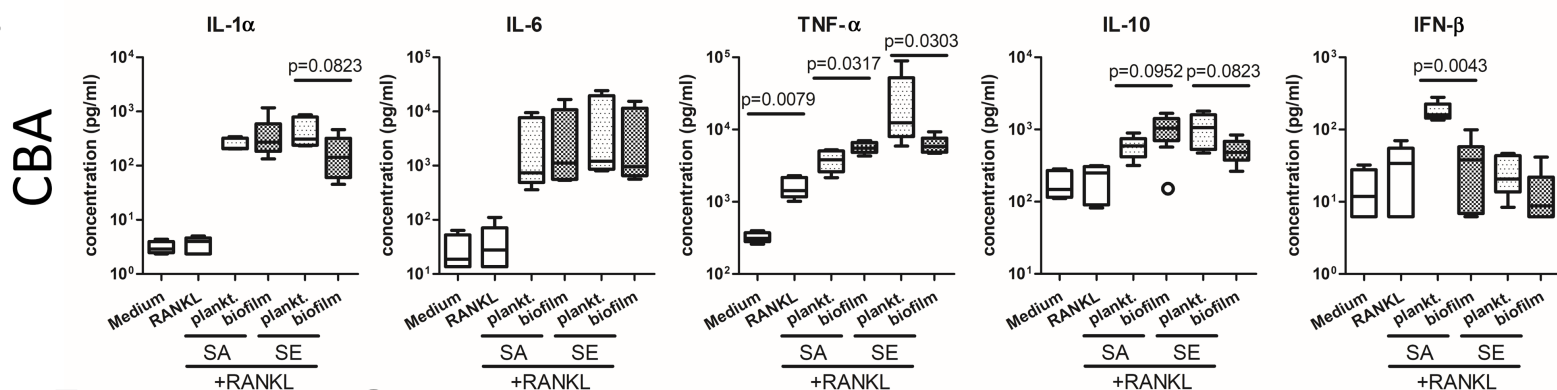
**C**



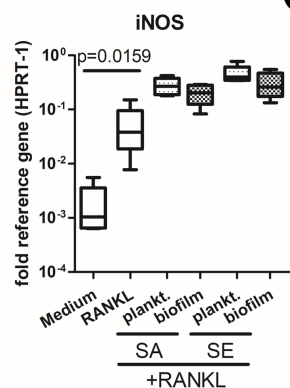
**D**



**E**



**F**



**G**

